AD NUMBER

AD802734

NEW LIMITATION CHANGE

TO

Approved for public release, distribution unlimited

FROM

Distribution authorized to U.S. Gov't. agencies and their contractors; Administrative/Operational Use; AUG 1966. Other requests shall be referred to Office of Naval Research, Arlington, VA 22203.

AUTHORITY

ONR notice dtd 27 Jul 1971

OBLIQUE FLOW HEADERS FOR HEAT EXCHANGERS— THE IDEAL GEOMETRIES AND THE EVALUATION OF LOSSES

By
A. L. London, G. Klopfer and S. Wolf

Technical Report No. 63

Prepared under Contract Nonr 225(91)
(NR-090-342)
for
Office of Naval Research

Department of Mechanical Engineering
Stanford University
Stanford, California

August 1966

OBLIQUE FLOW HEADERS FOR HEAT EXCHANGERS - THE IDEAL GEOMETRIES AND THE EVALUATION OF LOSSES

Technical Report No. 63

Prepared under Contract Nonr 225(91)
(NR-090-342)
for
Office of Naval Research

Department of Mechanical Engineering
Stanford University
Stanford, California

August, 1966

Report Prepared By:

A. L. London
G. Klopfer
S. Wolf

Approved By:

A. L. London
Project Supervisor

ABSTRACT

The problem of the design of oblique flow headers for heat exchangers flowing low density fluids is considered. It is demonstrated by test that the theory already available in the literature provides an adequate basis for design for the single-pass "parallel flow" and "counter flow" configurations. The theory is summarized in the form of design equations and illustrated by specific application to the air-side flow in a gas turbine regenerator.

TABLE OF CONTENTS

LIST OF TABLES

LIST OF FIGURES

NOMENCLATURE

English Letters

A	Flow area, ft^2
f	Flow friction factor in the exchanger matrix, dimensionless
g_c	Proportionality factor in Newton's Second Law = 32.2 (lbs/#)(ft/sec^2)
G	Flow mass velocity = velocity x ρ, lbs/hr ft^2
h	Velocity head = $\rho\, u_{ave}^2/2g_c$, #/ft^2, inches of water
KE	Flow stream kinetic energy rate ft #/sec
ℓ	Flow length through matrix, ft
L	Long dimension of header, ft
N_R	Reynolds No., dimensionless
p	Matrix porosity, flow void space/matrix vol., dimensionless
P	Fluid pressure, #/ft^2, inches of water
ΔP	Pressure drop, #/ft^2, psi, inches of water
r_h	Hydraulic radius for flow through the matrix, ft
t	The x-coordinate along the matrix face in Fig. 1-1
u	The fluid velocity component in the x-direction, ft/sec
v	The fluid velocity component in the y-direction, ft/sec
w	The fluid velocity along a stream line, ft/sec
x	Cartesian coordinate defined in Figs. 3 and 4, ft
X = x/L	
y	Cartesian coordinate defined in Figs. 3 and 4, ft
$Y = y_{wall}/y_o$	
z	Cartesian coordinate defined in Figs. 3 and 4, ft
$Z = z_{wall}/y_o$	

Greek Letters

α	Matrix friction area per unit volume, ft^2/ft^3
δ	On velocity means deviation from average
Δ	On pressure means pressure drop
ρ	Fluid density, lbs/ft^3
ω	Air flow rate, lbs/sec, lbs/hr

Subscripts

i Denotes inlet of inlet header

m Denotes matrix

o Denotes outlet of exit header

t Denotes "total" in distinction to static pressure, $P_t \triangleq P_{th}$.

ave Denotes average

Miscellaneous

lb Denotes pound mass in distinction to #

# Denotes pound force in distinction to lb

REFERENCES

1. S. Wolf, "Flow Losses for Heat Exchangers with Oblique Flow Headers," TR No. 60, Department of Mechanical Engineering, Stanford University, June, 1954.

2. M. Perlmutter, "Inlet and Exit Header Shapes for Uniform Flow Through a Resistance Parallel to the Main Stream," Trans. ASME, J. of Basic Engrg., 83, pp. 361-70, September, 1961.

3. J. F. Heyda, "An Analytical Study of a Balanced Reverse Folded Flow," XDC 60-1-158 General Electric Company Report, reprinted by Dept. of Commerce, Jan., 1960. See also the discussion of (2) by J. F. Heyda and C. D. Fulton.

4. A. L. Loeffler, Jr. and M. Perlmutter, "Turbulent Flow Through Porous Resistances Slightly Inclined to the Flow Direction," NACA TN 4221, 1958.

5. W. M. Kays and A. L. London, "Compact Heat Exchangers," 2nd Ed., McGraw-Hill Book Company.

INTRODUCTION

In energy conversion systems involving gas flow heat exchangers the header configurations have a definitive influence on system envelope geometry. The regenerative cycle gas turbine engine is an extreme example of such a system. The highly compact surfaces employed tend to result in cores of large frontal area and short flow length. The sketch, Fig. 1, illustrates a folded core concept used to reduce the header volume. However, if the pressure drop across the core is not uniform the flow distribution over the transfer surfaces will not be uniform and a serious reduction in heat exchanger performance may be the penalty.

From this viewpoint, the design objective for the header is to provide for acceptably uniform flow with acceptable system geometry and flow stream mechanical energy losses. In effect, uniformity of flow distribution is the dominating function of the headers.

The present report is a continuation of earlier work in this area described in Ref. (1). Three types of header configurations as shown in Fig. 2 are considered: a single-pass parallel flow, a single-pass counter flow and a two-pass parallel flow configuration. The specific purposes of this presentation are to:

(1) Summarize the analytical results, including a detailed analysis of losses, for the two single-pass configurations.

(2) Present test results for all three configurations, both for the "theory shaped" headers and for other shapes not conforming to the theory.

(3) To illustrate the application of the results by the design of a practical heat exchanger header.

The theoretical methodology is largely based on the work of Perlmutter and Heyda (2) and (3). The mathematical model for the exit header analysis differs for these two authors and the Heyda model is selected for the present treatment as

it is well substantiated experimentally. The analysis of header losses into inlet and exit components and the allowance for different fluid densities for the inlet and exit headers represent a simple, new contribution to the theory. It is believed that these extensions and the summary of results into convenient equations will be of value to the heat exchanger designer.

THEORY RESULTS

The mathematical models analyzed for the parallel flow and counter flow configurations are described in Figs. 3 and 4, respectively. The applicable idealizations follow:

1. Inlet and exit header densities are separately constant.
2. Inlet header velocity, u_i, is uniform at $x=0$.
3. The inlet header velocity is a function of x only.
4. The inlet header pressure is a function of x only.
5. The exit header pressure is a function of x only, but the velocity has a two-dimensional variation.
6. The inlet and exit header flows are loss free (inviscid).

The conditions imposed on the system are:

1. The exit header has a box shape

$$Y(X) = 1 \quad \text{or} \quad y_{wall}/y_o = 1$$

2. The mass flow distribution through the matrix is uniform, i.e., v_m = constant flowing into the exit header.
3. In order to provide for (2) it is necessary to shape the inlet header so that the inlet pressure profile $P(x)$ matches the exit pressure profile to make ΔP matrix constant with x (see Figs. 3 and 4).

The important results of the analysis are:

1. $P(x)$ for the exit header.
2. $u_o(y)$ for the exit header.
3. Required shape of the inlet header $Z(x)$.
4. $u(x)$ for the inlet header.

The details of the derivations are presented in APPENDIX I.

It is evident from the foregoing that the treatment is one-dimensionalized with respect to pressure in both headers and also velocity in the inlet header, but the outlet header velocity $u(x,y)$ is two-dimensional. As will be shown, the one-dimensional idealization for pressure is justified by experiment. The justification for selecting a box shape of the exit header is that it yields a minimum pressure drop,

Refs. (1, 2, 3).

Even though the flow in each of the headers is loss free, according to idealization (6), there is a header loss chargeable to the inlet and exit header and matrix system. This loss has two sources: (a) the kinetic energy dissipation as the flow leaves the inlet header at a fairly high velocity and is turned and decelerated by the matrix and (b) the kinetic energy "excess" in the exit header associated with the non-uniform velocity profile $u_o(y)$ shown in Fig. 3. The header loss is defined as the loss in the total pressure that is not chargeable to the matrix, namely

$$\frac{\Delta P_{\ell}}{h_i} \triangleq \frac{(P_{i,t} - P_{o,t}) - \Delta P_{matrix}}{h_i} \qquad (1)$$

As the average velocity term in the exit total pressure $P_{o,t}$ is based on a bulk average u_o, any non-uniformity in u_o will appear as a "bookkeeping" loss in kinetic energy.

The experimental evidence supporting these idealizations will be presented later.

The important analytical results for the single-pass parallel flow header configuration follow:

Exit header, box configuration $Y(X) = 1$

$$\text{Pressure,} \quad \frac{P_i - P(X)}{h_o} = \frac{\Delta P_{matrix}}{h_o} + \frac{\pi^2 X^2}{4} \qquad (2)$$

$$\text{Velocity,} \quad \frac{u_o}{u_{o,ave}} = \frac{\pi}{2} \sin\left(\frac{\pi}{2} \frac{y}{y_o}\right) \qquad (3a)$$

$$\frac{(u_o^3)_{ave}}{(u_{o,ave})^3} = \frac{\pi^2}{6} = 1.645 \qquad (3b)$$

Inlet header

$$\text{Pressure,} \quad \frac{P_i - P(X)}{h_i} = \frac{\pi^2}{4} X^2 \left|\frac{\rho_i}{\rho_o}\right| \left|\frac{z_i}{y_o}\right|^2 \qquad (4)$$

Geometry, $$Z = \frac{(1 - X)}{\left[\left(\frac{\rho_i}{\rho_o}\right)\left(\frac{\pi}{4}\right)^2 X^2 + \left(\frac{y_o}{z_i}\right)^2\right]^{1/2}} \qquad (5)$$

Velocity, $$\frac{u}{u_i} = \sqrt{\left(\frac{\rho_i}{\rho_o}\right)\left(\frac{z_i}{y_o}\right)^2 \frac{\pi^2}{4} X^2 + 1} \qquad (6a)$$

$$\frac{(u^2)_{ave}}{u_i^2} = 1 + \frac{\pi^2}{12}\left(\frac{\rho_i}{\rho_o}\right)\left(\frac{z_i}{y_o}\right)^2 = 1 + 0.822\left(\frac{\rho_i}{\rho_o}\right)\left(\frac{z_i}{y_o}\right)^2 \qquad (6b)$$

Note that from continuity

$$\frac{h_o}{h_i} = \left(\frac{\rho_i}{\rho_o}\right)\left(\frac{z_i}{y_o}\right)^2 \qquad (6c)$$

The mathematical model for the counter flow header configuration is described in Fig. 4. In contrast to the parallel flow configuration, the inlet header functions as a diffuser to decelerate the flow. The outlet header behaves exactly like that for the parallel flow configuration with a flow acceleration and a drop in pressure in the flow direction.

The important analytical results for the single-pass counter flow configuration follow:

Exit header, box configuration $Y(X) = 1$

Pressure, $$\frac{P_i - P(X)}{h_o} = \frac{\Delta P_{matrix}}{h_o} = \frac{\pi^2}{4}\left[1 - (1 - X)^2\right] \qquad (7)$$

Velocity, $$\frac{u_o}{u_{o,ave}} = \frac{\pi}{2}\sin\left(\frac{\pi}{2}\frac{y}{y_o}\right) \qquad (8a)$$

$$\frac{(u_o^3)_{ave}}{(u_{o,ave})^3} = \frac{\pi^2}{6} = 1.645 \qquad (8b)$$

Inlet header

Pressure, $$\frac{P(X) - P_i}{h_i} = \left(\frac{\rho_i}{\rho_o}\right)\left(\frac{z_i}{y_o}\right)^2 \frac{\pi^2}{4}\left[1 - (1 - X)^2\right] \qquad (9)$$

Geometry, $Z = \frac{2}{\pi}\sqrt{\frac{\rho_o}{\rho_i}} = 0.636\sqrt{\frac{\rho_o}{\rho_i}}$ (10)

(no box header is required)

Velocity, $\frac{u_i}{u_i} = (1 - X)$ (11a)

$$\frac{(u^2)_{ave}}{u_i^2} = \frac{1}{3} \quad (11b)$$

Note that from Eq. (10) and continuity

$$\frac{h_o}{h_i} = \left(\frac{\rho_i}{\rho_o}\right)\left(\frac{z_i}{y_o}\right)^2 = \frac{4}{\pi^2} = 0.405 \quad (11c)$$

In contrast to the parallel flow configuration, where the inlet header dimension z_i can be either larger or smaller than the outlet dimension y_o, for counter flow z_i must be $0.636\sqrt{(\rho_o/\rho_i)}\, y_o$ in order to assure the matching pressure profile needed for uniform flow distribution and for a minimum header loss. This point is established in the derivation of Eq. (I-22) in APPENDIX I.

In the following consideration the over-all loss of flow stream mechanical energy, Eq. (1), will be analyzed in terms of its two components: (a) the kinetic energy dissipation as the flow leaves the inlet header and (b) the kinetic energy "excess" associated with the non-uniform velocity profile $u_o(y)$, shown in Fig. 3, which is chargeable to the exit header.

For the parallel flow configuration from Eqs. (2) and (6c), Eq. (1) becomes

$$\frac{\Delta P_t}{h_i} = \left(\frac{h_o}{h_i}\right)\left[\frac{\pi^2}{4} + \frac{h_i}{h_o} - 1\right] = 1.467\left(\frac{\rho_i}{\rho_o}\right)\left(\frac{z_i}{y_o}\right)^2 + 1$$

$$= 1.467\,\frac{h_o}{h_i} + 1 \quad (12)$$

For the counter flow configuration, from Eqs. (7) and (11c), Eq. (1) becomes

$$\frac{\Delta P_t}{h_i} = 1 + \frac{h_o}{h_i} = 1 - \frac{4}{\pi^2} = 0.595 \qquad (13)$$

Two interesting design conclusions are immediately evident, namely: (a) the optimum counter flow configuration has the much smaller loss and (b) unlike the parallel flow situation the counter flow loss does not depend on inlet to outlet flow stream density ratio. A typical parallel flow design would be with

$$\left(\frac{z_i}{y_o}\right)^2 = \frac{\rho_o}{\rho_i} \quad \text{or} \quad h_o = h_i$$

So that $\Delta P_t/h_i = 2.467$; 4.15 times the comparable counter flow loss.

The kinetic energy associated with the non-uniform velocity profile $u_o(y)$ at the outlet header exit is the same for both the parallel and counter flow configurations.

$$\frac{KE_o}{\omega} = \frac{1}{y_o \rho_o u_{o,ave}} \int_0^{y_o} (\rho_o u_o) \frac{u_o^2}{2g_c}\, dy = \frac{1}{(u_{o,ave})} \frac{(u_o^3)_{ave}}{2g_c}$$

The "excess" kinetic energy head above the nominal magnitude evaluated using a bulk average velocity is

$$\frac{\text{Exit Loss}}{h_o} \triangleq \frac{\rho_o \text{ Excess } KE_o/\omega}{h_o} = \frac{(u_o^3)_{ave}}{(u_{o,ave})^3} - 1$$

$$= \frac{\pi^2}{6} - 1 = 0.645 \qquad (14)$$

where the numerical result comes from Eq. (3b).

For the inlet header, the loss is postulated to be all the kinetic energy leaving the header and entering the matrix where it is dissipated, with no pressure rise and appears as an increase of enthalpy of the flow.

$$\frac{KE_{inlet}}{\dot{m}} = \frac{1}{\rho_i \, L \, v_m} \int_o^L \rho_i \, v_m \, \frac{u^2}{2g_c} \, dx$$

But v_m = constant with x and so is ρ_i ; thus the inlet loss becomes

$$\frac{\text{Inlet Loss}}{h_i} = \frac{(u^2)_{ave}}{u_i^2} \qquad (15a)$$

By Eq. (6b), for the inlet header of the parallel flow configuration

$$\frac{\text{Inlet Loss}}{h_i} = 1 + 0.822 \left[\frac{\rho_i}{\rho_o}\right] \left[\frac{z_i}{y_o}\right]^2 = 1 + 0.822 \, \frac{h_o}{h_i} \qquad (15b)$$

By Eq. (11b), for the inlet header of the counter flow configuration

$$\frac{\text{Inlet Loss}}{h_i} = 0.333 \qquad (15c)$$

From Eqs. (14) and (15b) for the parallel flow configuration

$$\frac{\Delta P_t}{h_i} = 0.645 \left(\frac{h_o}{h_i}\right) + 1 + 0.822 \left(\frac{h_o}{h_i}\right) = 1.467 \left(\frac{h_o}{h_i}\right) + 1$$

$$= 1.467 \left[\frac{\rho_i}{\rho_o}\right] \left[\frac{z_i}{y_o}\right]^2 + 1$$

which is in agreement with Eq. (12).

Similarly, from Eqs. (14) and (15c) for the counter flow configuration and using Eq. (11c)

$$\frac{\Delta P_t}{h_i} = 0.645 \, \frac{h_o}{h_i} + 0.333$$

$$= 0.645 \times 0.405 + 0.333 = 0.595$$

which is in agreement with Eq. (13).

In summary, the postulated "loss free" flow theory for the headers provides expressions for the losses to be charged to the headers in the header-matrix complex. Eqs. (12) and

(13) provide the total header losses, and Eqs. (14), (15b), and (15c) provide the exit and inlet header contributions to the total losses.

A technically interesting special case of the parallel flow solutions is considered in APPENDIX II. This configuration is described as the oblique flow inlet, free discharge configuration, Fig. I-3. This header configuration is quite commonly encountered in air conditioning heat exchanger installations and may also be of interest in a gas turbine regenerator discharging straight into an exhaust stack. The discharge pressure is uniform for this situation so the inlet header must be shaped to yield a uniform pressure. This pressure match condition requires a triangular shape, with uniform velocity $u = u_i$,

$$\frac{z_{wall}}{z_i} = (1 - X) \tag{16}$$

The exit header loss is nil so that the $\Delta P_t/h_i$ is completely due to the inlet header and according to Eq. (1) and Eq. (I-26) of APPENDIX I becomes

$$\frac{\Delta P_t}{h_i} = 1 \tag{17}$$

In contrast to Eqs. (12) and (13), it is seen that the header loss for the oblique flow inlet, free discharge configuration is intermediate to the parallel flow and counter flow configuration.

EXPERIMENTAL RESULTS

After a brief description of the test system, data will be presented supporting the idealizations made in the analysis. A flow non-uniformity criterion will be developed and the actual header performance will be presented both in terms of pressure profiles, header total head losses and flow non-uniformity. Theory shaped headers will be considered and also designs that differ from the theory. The performance of a two-pass parallel flow configuration will also be presented to indicate the type of extrapolation one may make of the single-pass theory.

Test System

The flow system for the single-pass parallel flow configuration is described schematically in Fig. 5. Fig. 6 is a photograph of the general test arrangement for parallel flow and Fig. 7 is a photograph of the counter flow configuration.

The matrix arrangement consisting of two HEXCEL stiffenens and seven pads of five screens each is shown in Fig. 8. The stiffeners proved to be very effective in eliminating header shape distortions due to the screens bulging and sagging.

Eight header sets were tested. Four of these are single-pass parallel flow configurations, three are counter flow and one is a two-pass parallel flow configuration. The three configurations were previously described in Fig. 2. Table 1 provides the important dimensions for the headers, and Tables 2 and 3 provide the matrix information.

Additional information relating to the test system is in APPENDIX II.

Experimental Verification of Idealizations

For the box exit header, a verification of the idealizations (page 3) leading to the analytical results, Eqs. (2,3a, 3b) and (7,8a,8b), is provided by a comparison of the measured exit velocity profile with the theory prediction, Eq. (3a).

This is done in Fig. 9 and the agreement is excellent.

The validity of the idealization of pressure as a function of x only in both the inlet and exit headers is provided by a comparison of the narrow side-wall pressure tap readings with those of the bottom and top walls. The side wall taps are located at a plane about one-fourth of y_o from the matrix stiffener face for both the inlet and outlet headers. These comparisons are presented in the experimental pressure profile Figs. 10 by the different types of data points. The close agreement of the two sets of pressure readings strongly supports the uni-dimensional idealization for the pressure.

Flow Uniformity Criterion

Before presenting the header performance, it is necessary to specify a criterion that is descriptive of flow non-uniformity through the matrix. It is necessary that this criterion be readily evaluated from test results and be usable by the designer to estimate the heat transfer performance penalty due to the non-uriformity. Fig. 10 presents a typical set of pressure data. After the pressure profiles are plotted, the $\Delta P_{matrix}/h_i$ is read from the graph at 11 equally spaced abscissa values over the range $0 \leq X \leq 1$. The $\sqrt{\Delta P_{matrix}/h_i}$ is then calculated and $v_m/v_{m,ave}$ is formed as

$$\frac{v_m}{v_{m,ave}} = \frac{\sqrt{\Delta P_{matrix}/h_i}}{\sqrt{\Delta P_{matrix}/h_i}\Big|_{ave}}$$

The 11 ordinate trapezoid rule is used to form the $\sqrt{\Delta P_{matrix}/h_i}\Big|_{ave}$. The departure of $v_m/v_{m,ave}$ from unity is the velocity deviation from the average

$$\frac{\delta v_m}{v_{m,ave}} \triangleq \left| \frac{v_m}{v_{m,ave}} - 1 \right|$$

The average deviation of the velocity deviation is taken as

the criterion of non-uniformity.

$$\text{Flow non-uniformity} \triangleq \left(\frac{\delta v_m}{v_{m,ave}}\right)_{ave}$$

The trapezoid rule is again used to form this average.

To estimate the penalty in heat transfer performance associated with a specified non-uniformity, it is recommended that the flow distribution be treated as suffering a step change ($\pm$) equal to the non-uniformity magnitude.

Clearly the flow non-uniformity factor is a characteristic of the header and heat exchanger matrix system and not of the headers alone. If the matrix pressure drop is large relative to the pressure changes in the headers, the influence of the headers on flow distribution will be minor. In the case of the test system, the pressure change in the matrix is approximately $2\ h_i$ (see Table 3). This is of the same order of magnitude as the pressure changes in the headers and, as a consequence, header performance has an important influence on the flow non-uniformity factor. It is believed that this situation is typical of gas turbine plane regenerators and intercoolers and many other gas flow heat exchanger systems.

Header Performance

The eight header configurations tested are listed in the first column of Tabl. 4. The main test conditions and the header performance, as characterized by the loss $\Delta P_t/h_i$ and the flow non-uniformity $(\delta v_m/v_{m,ave})_{ave}$ are also tabulated. Representative graphs, Figs. 10-17, all for a nominal mass flow rate of 3000 lbs/hr, provide the pressure profiles and the associate matrix flow distribution. For all these tests, ρ_i/ρ_o can be treated as unity for comparison with the theory predictions.

The four single-pass parallel flow configuration tests will be considered first. The approach of the actual inlet

header shape for runs 50, 51, and 52, the so-called "theory" inlet shape, to the geometry specified by Eq. (5) for $z_i/y_o = 1$ and $\rho_i/\rho_o = 1$, is reported in Fig. 18. Departures on the order of 3 percent (of z_i) may be noted. This lack of agreement undoubtedly contributes to the non-uniformity magnitude, averaging† about 3.6 percent.

The reduced flow area in the regions of $X \approx 0.7$ was considered to be the main contributing factor (see Fig. 10) so for runs 22, 23, and 24 a 0.02-inch thick frame was used to produce the modified theory geometry reported in Fig. 19. The resulting non-uniformity was reduced to 2 percent. It is evident however from Fig. 11 that for $X > 0.9$ the flow area is too great so that $P(X)_{inlet}$ does not drop off enough to match the $P(X)_{outlet}$ profile in this region. It is believed on the basis of this evidence that a closer approach to the theory geometry of Eq. (5) would indeed provide for better flow uniformity. However, for most exchanger applications a non-uniformity factor of 5 percent would probably be acceptable; and this can be achieved if dimensions are maintained to $\pm$ 2 percent of z_i and care is taken not to block off the small flow area region for $X > 0.7$.

The outlet header pressure profile for the theory and modified theory inlets, Figs. 10 and 11, very closely match the theory prediction of Eq. (2); $\Delta P_{outlet}/h_i$ is very close to the $(\pi^2/4) = 2.47$ from Eq. (2). The header loss $\Delta P_t/h_i$ averages† out to be 2.30 which is 7 percent below the theory prediction of Eq. (12). This difference may be a boundary layer effect as there is evidently a trend upwards for $\Delta P_t/h_i$ with increasing flow rate. A flow rate of $\omega = 2000$ lbs/hr, run No. 50, corresponds to an inlet Reynolds No. (based on the hydraulic diameter of A_i) of approximately 90,000.

†In the following discussion where three test runs in a set are being evaluated arithmetic average values will be used.

The triangular header shape is described in Fig. 19. Runs 31, 32, and 33, in Table 4, show that the non-uniformity averages 10 percent, substantially poorer than the performance of the theory shape of 2 to 4 percent. Fig. 12 shows the pressure profiles and the velocity distribution. Clearly gross departures from the theory shapes result in serious flow non-uniformities and to accentuate this point with a box header, run 10 and Fig. 13, a 21 percent non-uniformity results. Note, however, that compensating somewhat for the non-uniformity of flow distribution through the matrix the header loss, $\Delta P_t/h_i$, is reduced substantially from the theory value of 2.47. This point illustrates the fallacy of using header loss as a criterion of design excellence. The lower loss is obtained only at the expense of the main function of the headers, namely, to provide for close to uniform flow through the heat exchangers.

The three single-pass counter flow configurations listed in Table 4 will now be considered. The situation with $z_i/y_o = A_i/A_o = 0.636$ represents the theory shape when $\rho_o/\rho_i = 1$, Eq. (10). As can be seen from the entries for runs Nos. 53, 54, and 55 the flow non-uniformity factor averages at 4 percent which is considered to be quite acceptable, and the header head loss is $\Delta P_t/h_i = 0.62$ in comparison to the theory prediction of 0.60, Eq. (13). Fig. 14 shows the flow distribution and pressure profiles typical for this header. The pressure drop in the outlet header $\Delta P_{outlet}/h_i = 1.03$. From the theory Eq. (7)

$$\frac{\Delta P_{outlet}}{h_i} = \left[\frac{\Delta P'_{outlet}}{h_o}\right]\left[\frac{h_o}{h_i}\right] = \left[\frac{\pi^2}{4}\right]\left[\frac{4}{\pi^2}\right] = 1.00$$

Thus the agreement is quite excellent.

The second set of data, runs 45, 46, and 47, serves to demonstrate the influence of departing from the theory specifications. The inlet header area is "oversized" by the ratio

$(0.713/0.636) - 1 = 12$ percent. As can be seen from Table 4 entries, the flow non-uniformity is increased from 4 to 6 percent. The outlet header drop $(\Delta P_{outlet}/h_i)$ is increased from 1.03 to 1.25, but when normalized relative to h_o becomes $(\Delta P_{outlet}/h_o) = (1/0.713)^2 \times 1.25 = 2.45$ which closely approximates the $\pi^2/4 = 2.47$ of the outlet header flow theory, Eq. (7). The header loss $(\Delta P_t/h_i) = 0.82$ when it is normalized relative to h_i, but as h_i is decreased by $(0.713/0.636)^2 - 1 = 26$ percent, ΔP_t is only increased by 5 percent.

The third set of data, runs 38, 39, and 40, illustrates the effect of a substantial oversizing by $(0.97/0.636) - 1 = 53$ percent. Now the average flow non-uniformity factor is significantly greater at 11.5 percent. The outlet header drop $(\Delta P_{outlet}/h_o) = (\Delta P_{outlet}/h_i)(h_i/h_o) = (2.46)(1.063) = 2.62$ and this is within 6 percent of the theory prediction of $\pi^2/4 = 2.47$. Clearly the theory boundary condition of $v_m = \underline{\text{constant}}$ is not approximated, but nevertheless the agreement is good. As a matter of interest the parallel flow situation with the triangular inlet header, runs 31, 32, and 33, show about the same non-uniformity factor (10.2 percent average) and $\Delta P_{outlet}/h_o = 2.47$ is also the same. A comparison of Figs. 12 and 16 reveals a strong similarity in the character of the non-uniform v_m distribution. The header loss for the oversized inlet, counter flow configuration, $(\Delta P_t/h_i) = 1.27$, but because of the lower h_i, in the ratio $(0.636/0.97)^2$, the ΔP_t is actually lower than for the theory shape by 14 percent. So again at the expense of the primary function of the header, namely uniformity of flow distribution, a lower loss may be realized.

The last header configuration listed in Table 4, run 49, is the two-pass parallel flow configuration with single-pass theory shaped inlets and box headers for each pass. Fig. 17 provides the pressure profiles and the flow distribution.

In comparison to the comparable single-pass configuration, run 51, the first-pass behavior remains essentially unchanged but the second-pass reveals a 20 percent lower loss with a one point increase in the non-uniformity from 4.2 to 5.2 percent. Before the tests, it was anticipated that the highly skewed velocity profile $u_o(y)$, see Fig. 9, entering the second pass would tend to (a) increase the non-uniformity significantly and (b) increase the head loss for the second-pass. The contrary resulted. The small increase noted for the non-uniformity may not be significant. The substantial reduction of head loss can be rationalized by the fact that of the $\Delta P_t/h_i = \pi^2/4 = 2.47$ predicted by the theory for the first pass, 0.645 (26 percent) is assigned to the exit header, Eq. (14), and this is really a "bookkeeping" loss of kinetic energy associated with the convention of using the bulk average velocity to calculate flow stream kinetic energy. Clearly most of this excess kinetic energy is not lost in the inlet header to the second pass. The heat exchanger designer will welcome this fortunate circumstance. It also suggests that for single-pass configurations substantial non-uniformity in the inlet header velocity profile can be tolerated and may even prove desirable!

Good experimental verification of the theory for the oblique flow inlet, free discharge configuration, Eqs. (16) and (17) is reported by Loeffler and Perlmutter (4) and these same results are reported in (2).

APPLICATION TO DESIGN

It is evident from the test results that Eqs. (2) to (6c) for the parallel flow and Eqs. (7) to (11c) for the counter flow configuration can be used as a basis for design. The test results of the theory shaped headers support both the idealizations of the analysis and the resulting design equations. Also the analysis of flow stream mechanical energy losses chargeable individually to the inlet and exit headers, Eqs. (12) to (15c) are supported by the test results. Moreover, the "off theory" header tests illustrate the type and magnitude of the penalty to be paid in terms of non-uniformity of flow over the heat exchanger surfaces.

The purposes of this section are to illustrate the header sizing procedure by a specific example and to discuss other design considerations.

In Ref. (5) an example is presented for the design of a cross-flow regenerator core for a 5000 hp gas turbine plant. The following relevant information is extracted from this example for the purpose of designing the headers for the compressor air flow which is heated on passing through the regenerator.

Regenerator effectiveness	$\epsilon = 75\%$
Air-side core pressure drop	$\Delta P/P_i = 0.42\%$
Air flow densities	$\rho_i = 0.438$ lbs/ft^3
	$\rho_o = 0.300$ lbs/ft^3
	$\rho_i/\rho_o = 1.46$
Matrix frontal area	$A_m = 3' \times 7.5' = 22.5$ ft^2
Air flow rate	ω=193,000 lbs/hr=53.7 lbs/sec
Inlet air pressure	$P_i = 132$ psia

For the single-pass parallel flow header design, it will be specified that the inlet header initial velocity $u_i = 100$ ft/sec and that the exit header will be sized so as to make $h_o = h_i$. Under these conditions

$$h_o = h_i = \rho_i \frac{u_i^2}{2g_c} = 68.0\ \#/ft^2 = 13.1\ "H_2O = 0.472\ \#/in^2$$

$$A_i = \frac{\omega}{u_i \rho_i} = 1.225\ ft^2$$

$$u_{o,ave} = \sqrt{2g_c h_o/\rho_o} = 121\ ft/sec$$

$$A_o = \frac{\omega}{\rho_o u_{o,ave}} = 1.48\ ft^2$$

$$A_i/A_o = 0.828$$

For the single-pass counter flow header design, it is only necessary to specify u_i, taken as before as 100 ft/sec. One cannot impose an arbitrary relationship between h_o and h_i as this condition is fixed by the theory Eq. (11c). In applying the theory the ratio z_i/y_o will be taken as equivalent to A_i/A_o. The implication is that the x-section of the headers need not be rectangular as specified in Figs. 3 and 4, representing the mathematical models. It is believed that this is a valid approximation for smoothly contoured header walls.

Parallel Flow Header

From Eq. (6c) with $h_o = h_i$

$$\left(\frac{\rho_i}{\rho_o}\right)\left(\frac{A_i}{A_o}\right)^2 = 1 \quad \text{and} \quad \frac{A_i}{A_o} = \sqrt{\frac{1}{1.46}} = 0.828$$

This checks the previously derived result.
Introducing Eq. (6c) into Eq. (5) yields

$$Z = \frac{(1 - X)}{\left(\frac{\rho_i}{\rho_o}\right)^{1/2}\left[\frac{\pi^2}{4} X^2 + \frac{h_i}{h_o}\right]^{1/2}}$$

With $h_i/h_o = 1$ the following tabulation for the header shape results

X	0	0.25	0.50	0.75	1.00
$Z = A_i/A_o$	0.828	0.577	0.324	0.134	0
A ft^2	1.225	0.855	0.480	0.198	0
x for L = 7.5 ft	0	1.875	3.75	5.62	7.5

The header loss may be evaluated from Eq. (12)

$$\frac{\Delta P_t}{h_i} = 1.47 \frac{h_o}{h_i} + 1 = 2.47$$

$$\frac{\Delta P_t}{P_i} = \frac{2.47 \times 0.472}{132} = 0.883\%$$

From Eq. (14) the exit header loss is $0.645\ h_o = 0.645\ h_i$; 26 percent of the total. From Eq. (15) the inlet header loss is $1.822\ h_i$ or 74 percent of the total.

Counter Flow Header

From Eq. (11c)

$$\frac{h_o}{h_i} = \frac{4}{\pi^2} = 0.405$$

With u_i specified as 100 ft/sec, $h_i = 68\ \#/ft^2$ so

$$h_o = 27.5\ \#/ft^2$$

$$\frac{u_o}{u_i} = \sqrt{\frac{h_o}{h_i}}\sqrt{\frac{\rho_i}{\rho_o}} = \sqrt{0.405}\sqrt{1.46} = 0.770$$

$$u_o = 77 \text{ ft/sec}$$

$$\frac{\rho_o u_o^2}{2g_c} = h_o = \frac{0.30 \times 77^2}{64.4} = 27.6\ \#/ft^2 \text{ (check)}$$

From Eq. (10)

$$Z = \text{constant} = \frac{A}{A_o} = \frac{A_i}{A_o} = 0.636\sqrt{\frac{\rho_o}{\rho_i}} = 0.526$$

For $A_i = 1.225$ ft^2 (with $u_i = 100$ ft/sec)

$A_o = 2.33$ ft^2

From Eq. (13)

$$\frac{\Delta P_t}{h_i} = 0.595$$

$$\frac{\Delta P_t}{P_i} = \frac{0.595 \times 0.472}{132} = 0.213\%$$

From Eq. (14) the exit header loss is $0.645\ h_o = 0.645 \times 0.405\ h_i = 0.261\ h_i$ or 44 percent of the total. From Eq. (15c) the inlet header loss is $0.333\ h_i$ or 56 percent of the total.

The parallel flow and counter flow designs are compared in the following tabulation.

		Parallel Flow	Counter Flow
Inlet velocity	u_i, ft/sec	100	100
Exit velocity	$u_{c,ave}$, ft/sec	121	77
Inlet area	A_i, ft^2	1.225	1.225
Exit area	A_o, ft^2	1.48	2.33
Inlet header area	$A(x)$	See tabulation, p. 19	Constant at A_i
Exit header area	$A(x)$	Constant at A_o	Constant at A_o
Header losses	$\Delta P_t/h_i$	2.47	0.595
	$\Delta P_t/P_i$, %	0.883	0.213
Fraction for inlet header, %		74	56
Fraction for outlet header, %		26	44

As a point of interest it is noted that for the parallel flow design the header loss of 0.88 percent exceeds the calculated heat exchanger surface pressure drop of 0.42 percent (Ref. (5), p. 256) by more than two-fold. It is also clear that the counter flow design though somewhat more bulky (see the A_o

comparison) is very much to be preferred if the machinery arrangement will allow this configuration.

Because the core pressure drop is small relative to the pressure changes in the headers, in the ratio of 0.42/0.88 = 0.48, the header performance can be expected to have a greater influence on the non-uniformity factor than for the tests, for example, where the ratio was on the order of 0.8. Consequently the designs summarized above can be expected to have larger flow non-uniformities of the order of 5 percent in comparison to the test results of 2 to 4 percent.

Moreover, for the parallel flow design the inlet header dimensions must adhere fairly closely to the theory, say $\pm$ 2 percent of A_i, as in Figures 18 and 19. For the exit header no such precision is required. Both box headers for the counter flow configuration are less sensitive to off-specification dimensions in terms of the non-uniformity factor.

Both designs can probably tolerate fairly non-uniform inlet velocity conditions without too much of a penalty in flow non-uniformity.

As a point of interest the inlet header for the theory counter flow system is functioning as a very high area ratio diffuser with only a 33.3 percent loss (67 percent efficiency), Eq. (15c).

It appears that the single-pass counter flow header theory could be used to design a sharp return bend for a relatively small loss of about 0.60 h_i by using a low resistance matrix such as HEXCEL (one or two inches flow length) to function as turning vanes.

The test performance of the <u>two-pass parallel flow</u> configuration indicates that the single-pass theory provides quite a good basis for design as indicated by the test flow non-uniformity factors of only about 5 percent. This is a result of the lack of sensitivity of header performance (second pass inlet) to a skewed inlet velocity profile.

SUMMARY AND CONCLUSIONS

The previous text deals with the design of single-pass header systems of the parallel flow and counter flow types. Both the theory and test results are presented. Based on this information the following conclusions result.

1. An adequate design basis for single-pass parallel flow and counter flow header configurations now exists; that is, optimum geometries can be specified, expected losses estimated and reasonably good flow distribution uniformity over the heat exchanger surfaces can be anticipated.
2. Parallel flow headers will have losses of the order of four times that of counter flow configurations.
3. The header performance is believed to be relatively insensitive to inlet velocity distribution. This tentative conclusion needs further experimental verification.
4. Close adherence to the theoretical shape is necessary for the parallel flow design but no such close tolerances are required for the counter flow configuration.
5. A two-pass parallel flow header can be designed using single-pass theory largely because of item (3).
6. The influence of flow non-uniformity on heat exchanger performance deterioration can be calculated in specific instances using an extension of the heat exchanger design theory presented in (5). Generally the penalty is greater for high design effectiveness, for C_{min}/C_{max} approaching unity and for situations where a "high" for one fluid stream is opposite a "low" for the other fluid stream.
7. Using the design basis presented in this report,

average deviations from flow uniformity can be expected to be better than ± 5 percent.

8. The oblique flow inlet, free discharge configuration described in APPENDIX I, Fig. I-3 may be of special interest to air conditioning as well as gas turbine heat exchanger designers. Header losses are intermediate to the counter flow and parallel flow configurations.

TABLE 1

HEADER GEOMETRIES

	z_i or y_o inches	A_i or A_o ft^2	$\frac{A_m}{A_i \text{ (or } A_c)}$	$\frac{A_i}{A_o} = \frac{z_i}{y_o}$
INLET HEADERS				
Theory shape (Fig. 18)	2.06	0.143	8.25	0.97
Modified theory shape (.020" frame) (Fig. 19)	2.08	0.144	8.17	0.98
Triangular (Fig. 19)	2.06	0.143	8.25	0.97
Box (0.636 ratio)	1.35	0.0938	12.60	0.636
Box (0.713 ratio)	1.51	0.105	11.25	0.713
Box (0.97 ratio)	2.06	0.143	8.25	0.97
EXIT HEADERS				
Box for parallel flow, counter flow and second pass of 2-pass parallel flow	2.12	0.147	(8.00)	
Box for first pass of 2-pass parallel flow	2.10	0.146	(8.10)	

TABLE 2

MATRIX GEOMETRY

No. of screen layers	35
Frontal area (17.0" x 10.0"), A_m ft^2	1.18
Mesh designation per inch	24 x 24.5
Wire diameter, inches	0.0135
Estimated porosity, p	0.725
area density, α ft^2/ft^3	980
hydraulic radius, r_h ft	0.740×10^{-3}
flow length, L ft	0.0787
L/r_h	106.5
(1) Flow area to header area ratio, p A_m/A_i	5.98
Stiffeners (HEXCEL) Flow length, inches	2 x 1.00
cell size, inches	1/8
wall, inches	0.002

TABLE 3

PREDICTED CORE PRESSURE DROP

Nominal Flow Rate, ω lbs/hr	2000	3000	4000
(1) Mass Velocity, G lbs/hr ft^2	2340	3500	4670
Reynolds No., N_R	157	235	314
(2) Friction factor, $f = \phi(N_R, p)$	0.61	0.53	0.48
(3) $\Delta P_{matrix}/h_i = f(\ell/r_h)(A_i/pA_m)^2$	1.82	1.58	1.43

(1) Based on p A_m as the flow area.

(2) From ref. (5), Fig. 7-9, p. 130.

(3) Based on $A_i = 0.143$ ft^2, see Table 1.

TABLE 5

SUMMARY OF TEST RESULTS

Header Description	Test No.	Flow Rate lbs/hr	Inlet Vel. Head h_1 "H_2O	Pressure Drops $\Delta P_{overall}/P_1$	$\Delta P_{matrix}/P_1$	$\Delta P_{outlet}/P_1$	$\Delta P_{t,headers}/P_1$	$\left(\frac{\delta V_m}{V_{m,ave}}\right)_{air}$ %
Parallel Flow "Theory" inlet and box exit. $A_1/A_o = 1$	50	1937	0.615	4.54	2.29	2.34	2.25	3.4
	51	3030	1.42	4.30	1.98	2.46	2.32	3.3
	52	3955	2.48	4.27	1.82	2.50	2.39	4.0
Parallel Flow "Theory" inlet +.020" spacer and box exit. $A_1/A_o = 1$	22	2000	0.637	4.46	2.26	2.35	2.29	1.9
	23	3015	1.45	4.30	2.06	2.52	2.24	1.8
	24	3970	2.53	4.26	1.90	2.56	2.36	2.2
Parallel Flow Triangular inlet and box exit. $A_1/A_o = 1$	31	2010	0.632	4.00	2.29	2.34	1.71	8.3
	32	3010	1.425	3.96	2.03	2.56	1.92	11.0
	33	4015	2.55	3.81	1.86	2.52	1.95	11.4
Parallel Flow Box inlet and box exit. $A_1/A_o = 1$	10	3000	1.42	3.50	1.97	2.75	1.53	21.0
Counter Flow Box inlet and box exit. $A_1/A_o = 0.636$	53	1992	1.42	1.00	0.93	0.97	0.615	3.0
	54	3010	3.28	0.90	0.88	1.03	0.615	4.4
	55	4005	5.91	0.84	0.81	1.06	0.625	4.6
Counter Flow Box inlet and box exit. $A_1/A_o = 0.713$	45	2005	1.162	1.58	1.28	1.23	0.80	4.5
	46	3015	2.64	1.40	1.08	1.23	0.82	6.2
	47	3985	4.68	1.35	1.02	1.30	0.83	6.4
Counter Flow Box inlet and box exit. $A_1/A_o = 0.97$	38	2015	0.635	3.44	2.22	2.37	1.22	9.8
	39	2997	1.417	3.20	1.92	2.45	1.28	11.6
	40	3985	2.53	3.13	1.83	2.55	1.30	13.1
~~2-Pass Parallel Flow First pass: "Theory" inlet and box exit. Second pass: "Theory" inlet and box exit.~~	~~48~~	~~2000~~	~~0.618~~	~~4.57~~				
2-Pass Parallel Flow First pass: "Theory" inlet and box exit. Second pass: "Theory" inlet and box exit.	48	2000	0.618	4.57(1)	2.26	2.31	2.31	4.5
				4.05(2)	2.27	2.28	1.78	5.1
	49	3012	1.42	4.27(1)	1.98(1)	2.38(1)	2.29(1)	4.2(1)
				3.78(2)	1.92(2)	2.36(2)	1.86(2)	5.2(2)

(1) First pass only.

(2) Second pass only.

Fig. 1

A folded core concept involving oblique flow headers.

Fig. 2

The single-pass parallel flow, single-pass counter flow and two-pass parallel flow configurations.

Fig. 3

The mathematical model for the single-pass parallel flow configuration.

Fig. 4

The mathematical model for the single-pass counter flow configuration.

FIGURE 1

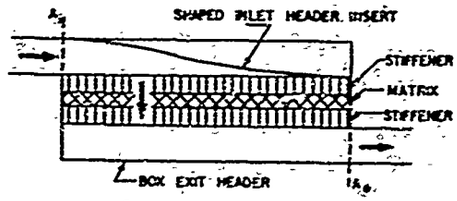

PARALLEL FLOW

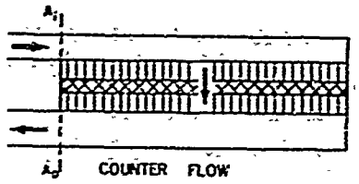

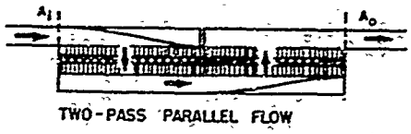

FIGURE 2

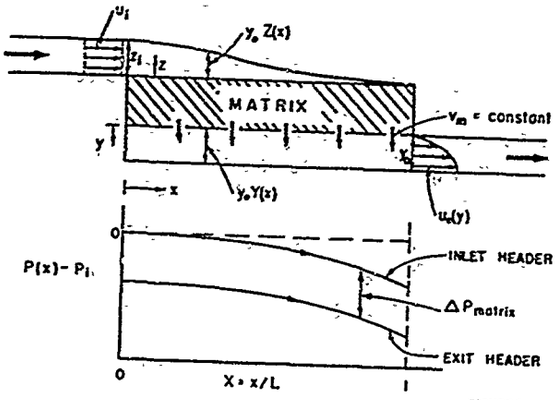

FIGURE 3

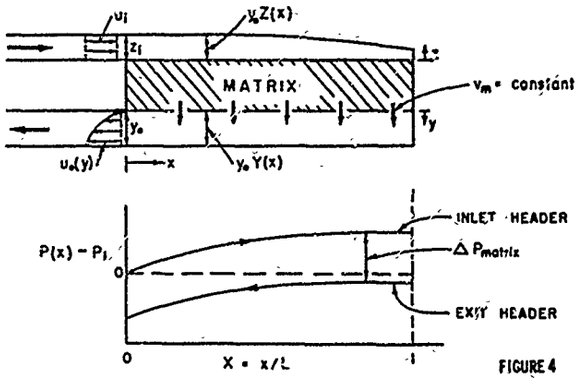

FIGURE 4

Fig. 5

The test system flow diagram. All dimensions are in inches.

Fig. 6

General view of the test system for the parallel flow experiments.

Fig. 7

The header and ducting test systems arrangement for the counter flow experiments.

Fig. 8

The screen matrix and the HEXCEL stiffeners.

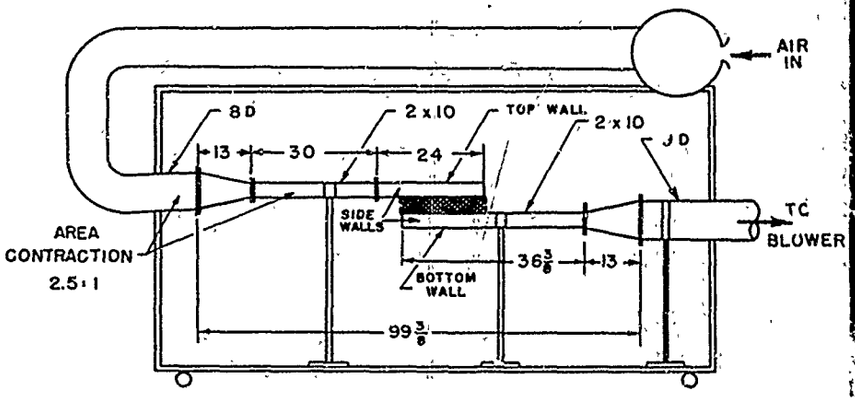

FIGURE 5

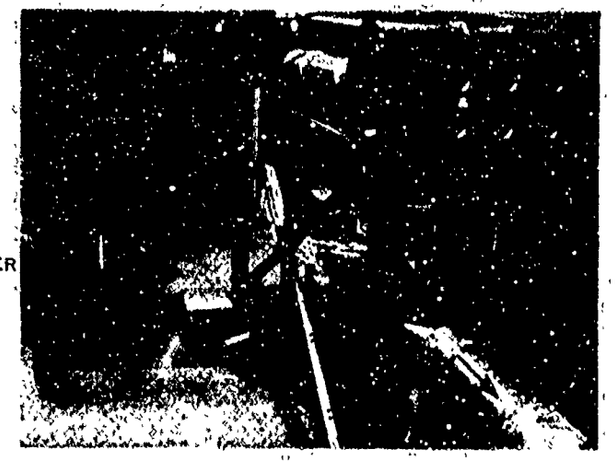

FIGURE 6

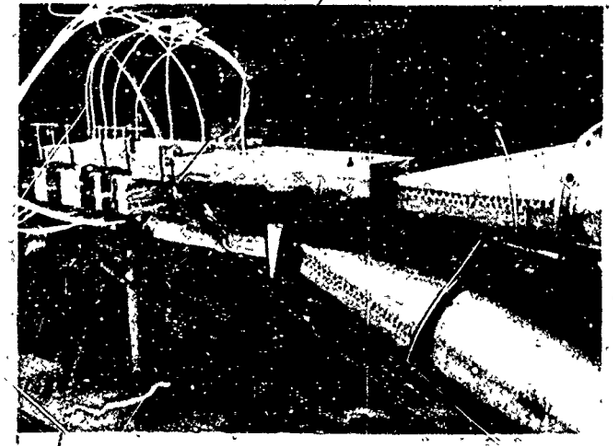

FIGURE 7

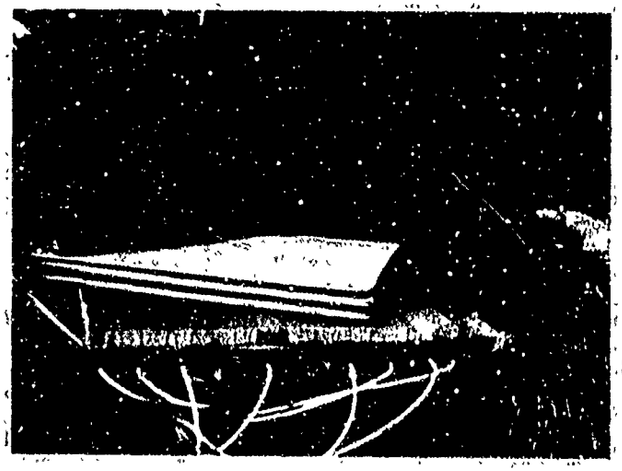

FIGURE 8

Fig. 9

The skewed velocity profile at the exit of the outlet of the theory shaped box header, Eq. (3a), compared with test results.

Fig. 10

Header performance for the theory shaped single-pass parallel flow configuration at ω = 3030 lbs/hr. Run No. 51. See Table 4 and Fig. 18 for other details. Note the one-dimensional behavior of P.

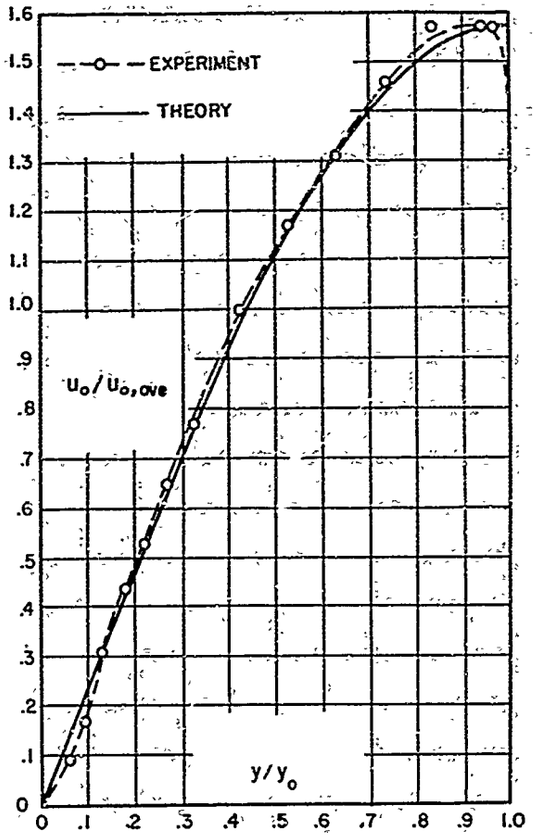

FIGURE 9

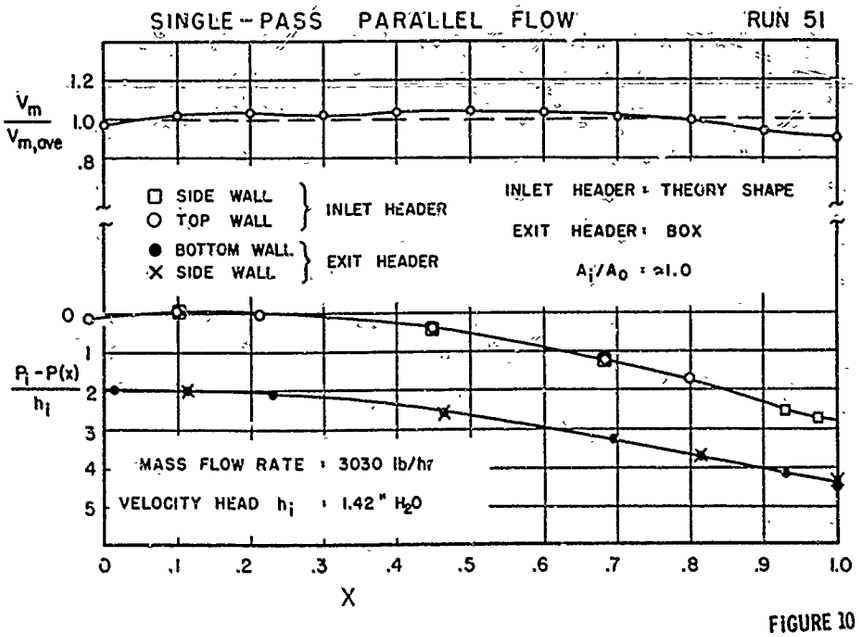

FIGURE 10

Fig. 11

Header performance for the modified theory shaped single-pass parallel flow configuration at ω = 3015 lbs/hr. Run No. 23. See Table 4 and Fig. 19 for other details.

Fig. 12

Header performance for the triangular shaped inlet single-pass parallel flow configuration at ω = 3010 lbs/hr. Run No. 32. See Table 4 and Fig. 19 for other details.

Fig. 13

Header performance for the box shaped inlet single-pass parallel flow configuration at ω = 3000 lbs/hr. Run No. 10. See Table 4 for other details.

Fig. 14

Header performance for the theory shaped A_i/A_o = 0.636, single-pass counter flow configuration at ω = 3010 lbs/hr. Run No. 54. See Table 4 for other details.

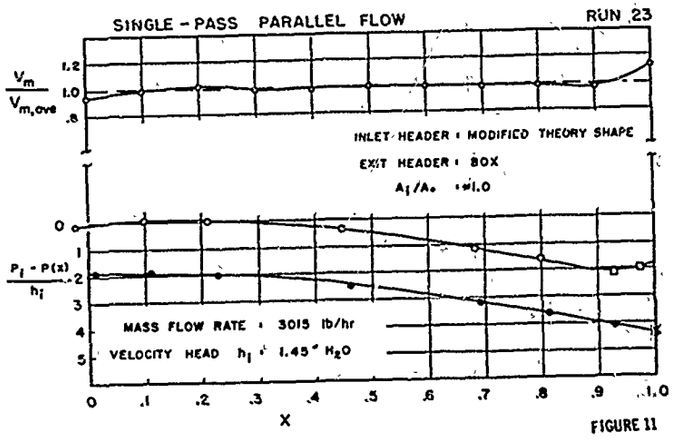

FIGURE 11

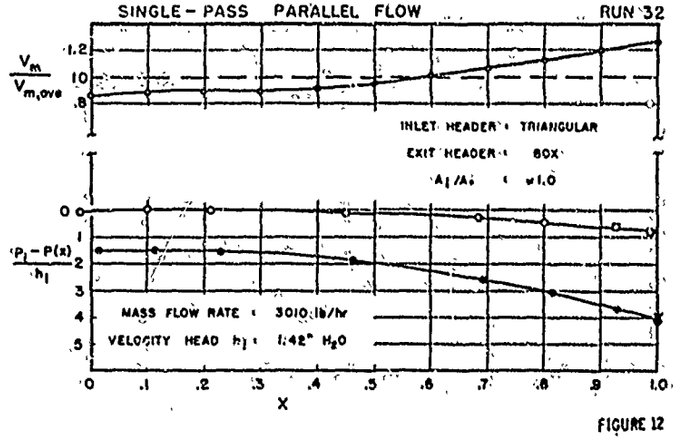

FIGURE 12

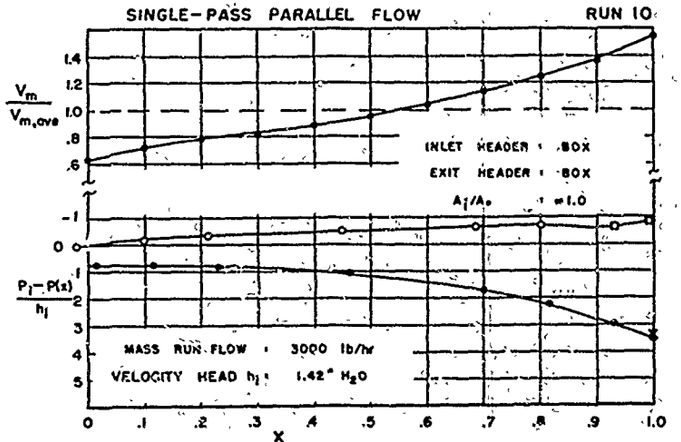

FIGURE 13

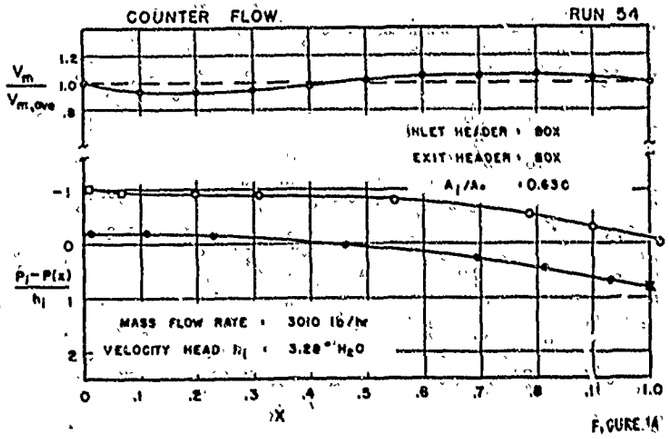

FIGURE 14

Fig. 15

Header performance for the oversized, $A_i/A_o = 0.713$, single-pass counter flow configuration at $\omega = 3015$ lbs/hr. Run No. 46. See Table 4 for other details.

Fig. 16

Header performance for the very much oversized, $A_i/A_o = 0.97$, single-pass counter flow configuration at $\omega = 2997$ lbs/hr. Run No. 39. See Table 4 for other details.

Fig. 17

Header performance for the two-pass parallel flow configuration with headers shaped according to single-pass theory at $\omega = 3012$ lbs/hr. Run No. 49. See Table 4 for other details.

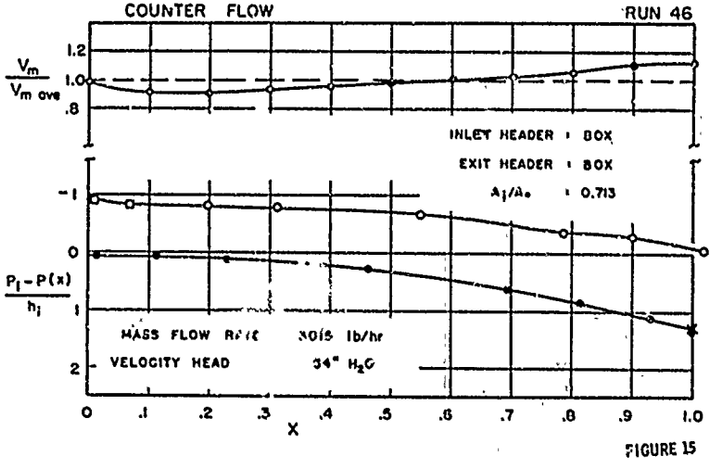

FIGURE 15

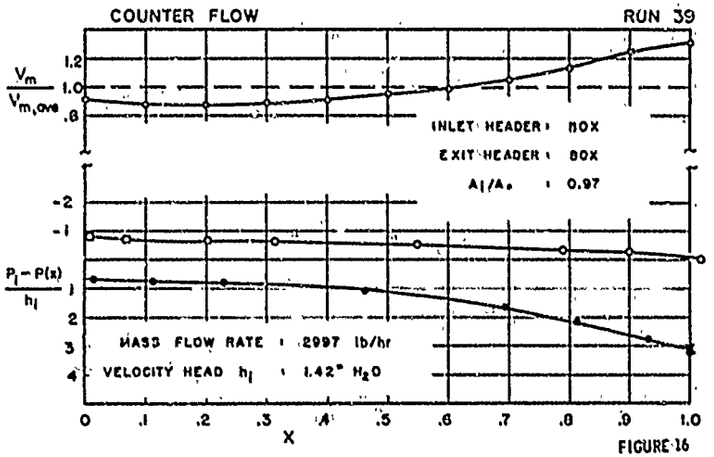

FIGURE 16

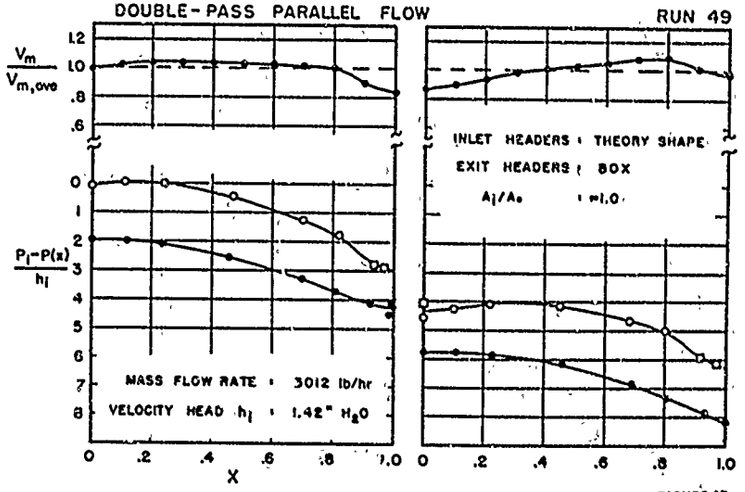

FIGURE 17

Fig. 18

Actual geometry of inlet header used in runs 50, 51 and 52 compared to the theory Eq. (5). See Table 1 for other details.

Fig. 19

Actual geometry of the inlet header of Fig. 18 modified with a 0.020 inch frame as used in runs 22, 23, and 24. Also the geometry of the triangular shaped inlet header as used in runs 31, 32 and 33.

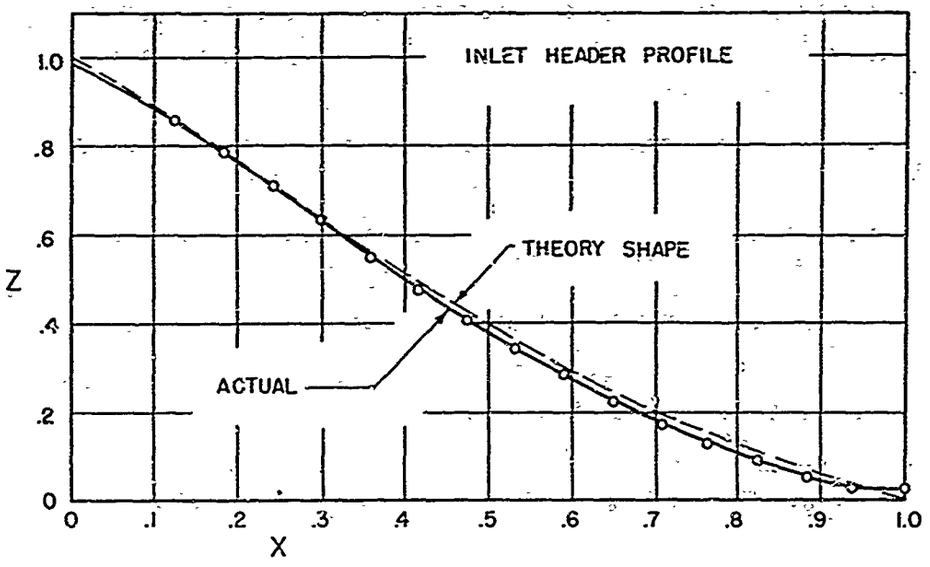

X	0	.1	.2	.3	.4	.5	.6	.7	.8	.9	1.0
Z	1.0	.89	.76	.63	.51	.39	.29	.20	.12	.06	0

FIGURE 18

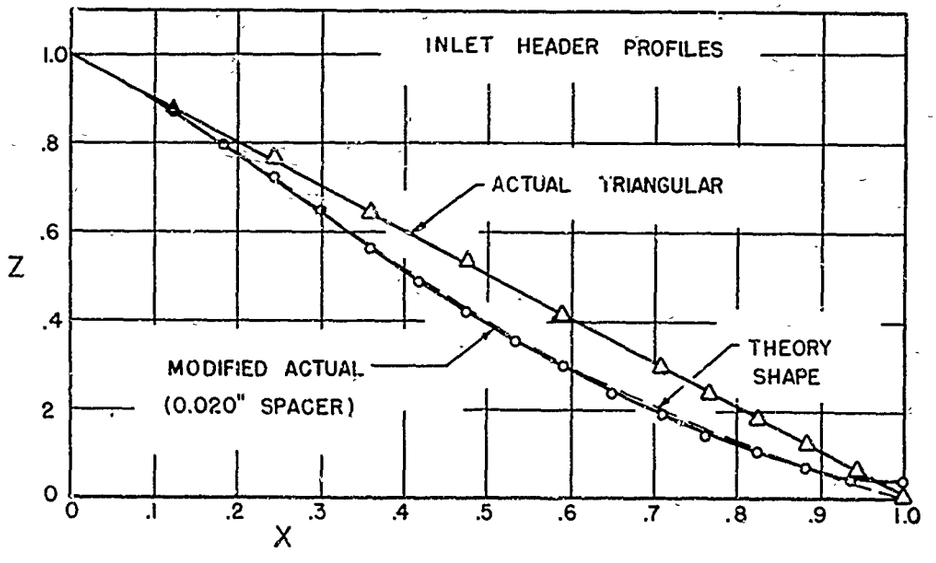

FIGURE 19

APPENDIX I

ANALYSIS OF OBLIQUE FLOW MODELS

The analysis presented here was first developed by Heyda (3) for the counter flow configuration. This method of analysis was then used by Wolf (1) for the parallel flow configuration. The repetition in this appendix is for the purpose of summarizing the two solutions and the methodology, using a uniform nomenclature, for the convenience of the reader.

The header models analyzed are described in Figs. I-1 and I-2. The outlet header analysis will apply to both configurations and will be given first. Then the inlet header for the parallel flow configuration will be analyzed followed by the inlet header for the counter flow configuration.

The outlet shape is specified as rectangular

$$Y(X) = 1$$

and the pressure profile is derived for a uniform velocity leaving the matrix, assuming pressure a function of X only, but allowing the streamline velocity to be a function of x and y. Then the inlet header shape is selected to provide a $P(X)$ which matches the exit header profile thereby maintaining a constant ΔP_{matrix} and a uniform flow distribution (v_m = constant) through the matrix, see Figs. 3 and 4.

Outlet Header

When the Navier-Stokes equations are expanded for steady, constant density, inviscid flow, the y-gradient of the pressure may be expressed

$$-\frac{\partial P}{\partial y} = \frac{\rho_o}{g_c}\left[u\,\frac{\partial v}{\partial x} + v\,\frac{\partial v}{\partial y}\right] \qquad \text{(I-1)}$$

But as P is specified to be a function of x only, the y-pressure gradient is zero, and this condition imposed on

Eq. (I-1) leads to

$$v = \text{constant } (=v_m) \qquad \text{(I-2)}$$

The Navier-Stokes equations may also be integrated along the streamline originating at point t of Figs. I-1 and I-2 to yield the Bernoulli equation for incompressible flow

$$P(x) + \frac{\rho_o}{2g_c}(u^2 + v^2) = P(t) + \frac{\rho_o}{2g_c} v_m^2$$

In light of Eq. (I-2) this reduces to

$$P(t) - P(x) = \rho_o \frac{u^2}{2g_c} \qquad \text{(I-3)}$$

From the conservation of matter principle, for density a constant, applied to the stream tube bounded by the streamlines originating at t and $t + dt$ † (using the coordinates of Fig. I-1)

$$-(u\,dy) = v_m dt \qquad \text{(I-4)}$$

Using this result for u and substituting into Eq. (I-3) yields

$$-dy = v_m \sqrt{\rho_o/2g_c} \frac{dt}{\sqrt{P(t) - P(x)}} \qquad \text{(I-5)}$$

This equation may be integrated to yield the wall contour $y_{wall}(x)$ by integrating between the limits

$$\text{for} \quad t = 0, \; y = y_{wall}(x)$$

$$\text{for} \quad t = x, \; y = 0$$

Thus,

$$y_{wall}(x) = \int_{y_{wall}(x)}^{0} -dy = \int_0^{t=x} v_m \sqrt{\rho_o/2g_c} \frac{dt}{\sqrt{P(t) - P(x)}} \qquad \text{(I-6)}$$

† Also $v_m L = u_{o,ave}\, y_o$.

This is a Volterra improper integral equation which has been solved by Hebya for some simple header shapes, $y_{wall}(x)$ (3). For the box header shape† considered here y_{wall} is constant and the solution yields

$$P(x=0) - P(x) = \frac{\pi^2}{4}\left(\rho_o \frac{u_{o,ave}^2}{2g_c}\right)\left(\frac{x}{L}\right)^2$$

$$= \frac{\pi^2}{4} h_o x^2 \qquad \text{(I-7)}$$

If the origin for x is taken at the outlet header section farthest away from the exit, this result will apply for the outlet box header for both the parallel and counter flow configurations Figs. I-1 and I-2.

With the pressure profile known one can determine the exit velocity u_o as a function of $y_{x=L}$ (Fig. I-1 coordinates). From the Bernoulli equation (I-3)

$$P(t) - P(L) = \rho_o \frac{u_o^2}{2g_c} \qquad \text{(I-8)}$$

But

$$P(t) - P(L) = \left\{[P(0) - P(L)] - [P(0) - P(t)]\right\}$$

$$= \frac{\pi^2}{4} h_o - \frac{\pi^2}{4} h_o \left(\frac{t}{L}\right)^2$$

$$= \frac{\pi^2}{4} h_o \left[1 - \left(\frac{t}{L}\right)^2\right] \qquad \text{(I-9)}$$

from Eq. (I-7). Equating (I-8) and (I-9)

$$\frac{u_o}{u_{o,ave}} = \frac{\pi}{2}\sqrt{1 - \left(\frac{t}{L}\right)^2} \qquad \text{(I-10)}$$

---

†The box header provides the smallest pressure drop for a given exit area.

Introducing u_o from the continuity equation (I-4), separating variables and integrating

$$-\int_{y_o}^{y} dy_{x=L} = \frac{2}{\pi}\frac{y_o}{L}\int_{o}^{t}\frac{dt}{\sqrt{1-\left(\frac{t}{L}\right)^2}}$$

The result is

$$\frac{y_{x=L}}{y_o} = \left[1 - \frac{2}{\pi}\sin^{-1}\frac{t}{L}\right] \qquad \text{(I-11)}$$

Solving for (t/L) and substituting in Eq. (I-10) yields the desired exit velocity u_o as a function of $y_{x=L}$

$$\frac{u_o}{u_{o,ave}} = \frac{\pi}{2}\cos\frac{\pi}{2}\left(1 - \frac{y}{y_o}\right) = \frac{\pi}{2}\sin\left(\frac{\pi}{2}\frac{y}{y_o}\right) \qquad \text{(I-12)}$$

This equation may be used to relate the actual exit kinetic energy rate to the nominal value calculated from the bulk average velocity. The result is

$$\frac{(KE_o/\omega)_{actual}}{(h_o/\rho_o)} = \frac{(u_o^3)_{ave}}{(u_{o,ave})^3} = \frac{\pi^2}{16}\left[\frac{\sin 3\theta}{3} + 3\sin\theta\right]_o^{\pi/2}$$

$$= \frac{\pi^2}{6} = 1.645 \qquad \text{(I-13)}$$

where $\theta \triangleq \frac{\pi}{2}\left(1 - \frac{y}{y_o}\right)$.

Equations (I-7), (I-12), and (I-13) are the important results for the exit box header used for both the single-pass parallel flow and counter flow configurations. The idealizations and specifications involved are as follows:

1. Constant density flow, $\rho = \rho_o$.
2. The flow through the matrix is uniform, v_m = constant.
3. Pressure is a function of x only.
4. Zero flow stream mechanical energy dissipation.

Inlet Header, Parallel Flow

For this analysis it is idealized that pressure and velocity are essentially functions of x only and that the density is constant. Then the Bernoulli equation for loss-free flow when applied to the streamline of Fig. I-1 is

$$P_i - P(x) = \frac{\rho_i}{2g_c}(u^2 - u_i^2) \qquad \text{(I-14)}$$

For constant density flow the conservation of matter principle provides the following relations for a uniform input velocity, u_i = constant , and uniform flow distribution through the core, v_m = constant .

$$\left.\begin{aligned} u_i z_i &= uz_{wall} + v_m x = v_m L \\ uz_{wall} &= v_m(L - x) \\ u_i z_i \rho_i &= u_{o,ave}\, y_o\, \rho_o \end{aligned}\right\} \qquad \text{(I-15)}$$

The pressure profile of Eq. (I-14) is required to match that of the exit header Eq. (I-7). So

$$P_i - P(x) = \frac{\pi^2}{4} h_o \left(\frac{x}{L}\right)^2 \qquad \text{(I-16)}$$

Combining Eqs. (I-16), (I-15), and (I-14) to eliminate P and u provides the desired inlet header shape z_{wall} as a function of x .

$$\left(\frac{\rho_i}{\rho_o}\right)\left(\frac{\pi^2}{4} X^2\right) = \left[\frac{(1 - X)^2}{Z^2} - \left(\frac{y_o}{z_i}\right)^2\right]$$

or

$$Z^2 = \frac{(1 - x)^2}{\left(\frac{\rho_i}{\rho_o}\right)\left(\frac{\pi^2}{4}\right) X^2 + \left(\frac{y_o}{z_i}\right)^2} \qquad \text{(I-17)}$$

where $Z \triangleq z_{wall}/y_o$ and $X \triangleq x/L$.

Note that

$$\frac{h_o}{h_i} = \left(\frac{\rho_i}{\rho_o}\right)\left(\frac{z_i}{y_o}\right)^2$$

Substitution of the header shape back into the continuity equation (I-15) will yield the inlet header velocity as a function of x

$$\frac{u}{u_i} = \sqrt{\frac{\rho_i}{\rho_o}\left(\frac{z_i}{y_o}\right)^2 \frac{\pi^2}{4} x^2 + 1} \qquad \text{(I-18)}$$

This relation may be used to establish the kinetic energy per unit mass of the flow leaving the inlet header and passing into the core.†

$$\frac{KE}{\omega} \triangleq \frac{1}{v_m \rho_i L} \int_o^L \frac{u^2}{2g_c} \rho_i v_m \, dx \qquad \text{(I-19a)}$$

The result is

$$\frac{(KE/\omega)}{(h_i/\rho_i)} = 1 + \frac{\pi^2}{12}\left(\frac{z_i}{y_o}\right)^2\left(\frac{\rho_i}{\rho_o}\right) = 1 + 0.822\left(\frac{z_i}{y_o}\right)^2\left(\frac{\rho_i}{\rho_o}\right) \qquad \text{(I-19b)}$$

Note the difference relative to Eq. (I-13) where the kinetic energy term involves a $(u^3)_{ave}$ instead of a $(u^2)_{ave}$ as above.

The important results for the inlet header in the single pass parallel flow configuration are Equations (I-16), (I-17), (I-18), and (I-19b). The idealizations and specifications involved are as follows:

1. Constant density flow, $\rho = \rho_i$ = constant.
2. Both pressure and velocity are essentially functions of x only.
3. Zero flow stream mechanical energy dissipation.

---

†Note that v_m in Eq. (I-19a) is the matrix velocity based on A_m at the inlet face of the matrix, in contrast to the v_m pictured in Fig. I-1 which is the matrix velocity at the outlet face.

4. The flow through the matrix is uniform, v_m = constant.
5. The entering flow is of uniform velocity, u_i = constant.
6. The pressure profile matches that of the exit box header.

Inlet Header, Counter Flow

For this analysis, as for the parallel flow inlet header, it is idealized that pressure and velocity are essentially functions of x only and that the density is constant. Then the Bernoulli equation for loss-free flow applied to the streamline indicated in Fig. I-2 is the same as (I-14). Also from the conservation of matter principle the (I-15) set of equations apply. However, in order to satisfy a pressure match with the exit header, Eq. (I-7) requires a shift in coordinates because of the counter flow configuration. The pressure profile then becomes

$$P(x) - P_i = \frac{\pi^2}{4} h_o \left[1 - (1 - X)^2\right] \qquad \text{(I-20)}$$

That is the inlet header now has to function as a diffuser with a flow deceleration in contrast to the parallel flow situation where the flow is accelerated. Combining the Bernoulli equation (I-14) with continuity, Eq. (I-15), and the pressure match condition, Eq. (I-20), so as to eliminate P and u provides the desired inlet shape z_{wall} as a function of x .

$$Z^2 = \frac{(1 - X)^2}{\left(\frac{y_o}{z_i}\right)^2 - \left(\frac{\rho_i}{\rho_o}\right)\left(\frac{\pi^2}{4}\right)\left[1 - (1 - X)^2\right]} \qquad \text{(I-21)}$$

To avoid imaginary values for Z it is necessary that the denominator of Eq. (I-21) be positive or

$$\left(\frac{y_o}{z_i}\right)^2 \geq \left(\frac{\rho_i}{\rho_o}\right)\left(\frac{\pi^2}{4}\right)\left[1 - (1 - X)^2\right]$$

The maximum value of the right hand side is $(\rho_i/\rho_o)(\pi^2/4)$ for $X = 1$. So

$$\left.\frac{z_i}{y_o}\right|_{max} = \frac{2}{\pi}\sqrt{\rho_o/\rho_i} = 0.637\sqrt{\rho_o/\rho_i}$$

Following Heoya (3), this value for z_i/y_o will be accepted as the "economic size" as smaller magnitudes would have a higher h_i and higher losses of kinetic energy when the flow enters the matrix. When this optimum (z_i/y_o) magnitude is introduced into Eq. (I-21) the optimum header shape becomes

$$Z^2 = \left(\frac{4}{\pi^2}\right)\frac{\rho_o}{\rho_i} = \text{constant} \qquad \text{(I-22)}$$

That is the optimum inlet shape is also a box header.

Substitution of this header shape back into the continuity equation (I-15) yields the inlet header velocity as a function of x

$$\frac{u}{u_i} = 1 - X \qquad \text{(I-23)}$$

Following the procedure used in establishing Eq. (I-19b) the kinetic energy per unit mass leaving the inlet header and passing into the core is

$$\frac{KE_i/\omega}{(h_i/\rho_i)} = \frac{(u^2)_{ave}}{u_i^2} = \frac{1}{3} \qquad \text{(I-24)}$$

The important results for the inlet header in the single pass counter flow configuration are equations (I-20), (I-22), (I-23) and (I-24). The idealizations and specifications involved are the same as for the inlet header for the parallel flow configuration and are listed following Eq. (I-19b).

Oblique Flow Inlet, Free Discharge

A technically interesting variation of the parallel flow configuration is pictured in Fig. I-3. If the outlet header is made very deep, $(y_o \to \infty)$, the outlet pressure profile becomes

uniform. This is also the situation for the free discharge configuration shown in Fig. I-3. This header configuration is quite commonly found in air conditioning exchangers where the free discharge of the conditioned air is directed into the room. It would also be the situation on the hot gas side of a gas turbine regenerator discharging straight up an exhaust stack. Under these circumstances Eq. (I-17) for the inlet header shape reduces to

$$\frac{z_{wall}}{z_i} = (1 - X) \qquad \text{(I-25)}$$

That is a triangular shape. This solution is the same as presented by Loeffler and Perlmutter (4).

This result can also be derived directly from the Bernoulli equation (I-14), and conservation of matter equation (I-15) and the pressure profile matching condition. From Eq. (I-14) and the pressure profile matching condition, $P(x) = \text{constant}$

$$u = u_i = \text{constant}$$

Then from the second of Eqs. (I-15)

$$\frac{z_{wall}}{z_i} = \frac{v_m L(1 - X)}{u\, z_i} = \frac{v_m L(1 - X)}{u_i\, z_i}$$

Introducing $u_i z_i = v_m L$ from the first of Eqs. (I-15) yields Eq. (I-25).

From Eq. (I-19a), the defining equation for KE/ω,

$$\frac{(KE/\omega)}{(h_i/\rho_i)} = 1 \qquad \text{(I-26)}$$

This also comes directly from Eq. (I-19b) for $y_o \to \infty$.

Fig. I-1

The mathematical model for the single-pass parallel flow configuration showing the stream line analyzed.

Fig. I-2

The mathematical model for the single-pass counter flow configuration showing the stream line analyzed.

Fig. I-3

The oblique flow inlet, free discharge model as a limiting case of the parallel flow configuration.

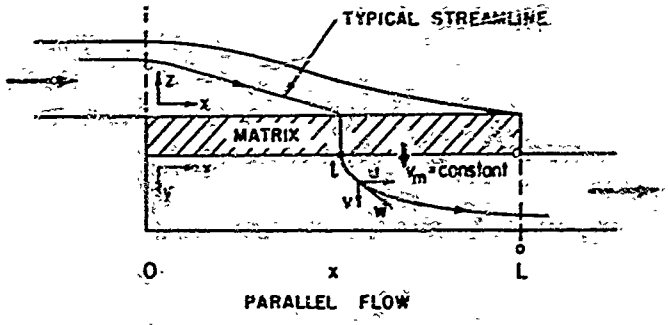

FIGURE I-1

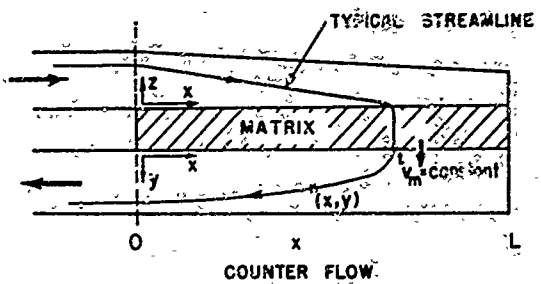

FIGURE I-2

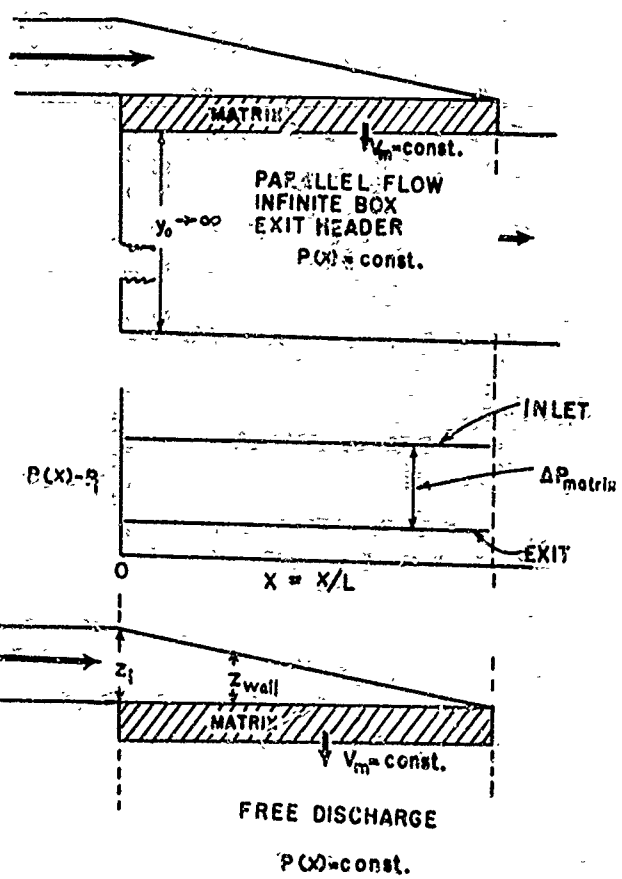

FIGURE I-3

APPENDIX II

FURTHER COMMENTS ON THE TEST SYSTEM

The test system was described in the text, Tables 1 to 3 and in Figs. 5 to 8 and 18 and 19. The purposes of this appendix are to describe some of the details of construction and to discuss some of the details of test data evaluation.

Header Construction

The headers consisted of a box sheet metal shell with replaceable wooden inserts used to provide the desired geometry. These are pictured in the photographs Figs. II-1 and II-2.

The narrow side-wall pressure taps were located on one of the two side walls as shown in Fig. II-2. The pressure taps along the broad wall consisted of brass tubes pressed through holes in the wood and the sheet metal. The 1/8-inch outer diameter tube end was finished flush with the contoured wooden surface. A strip of thin transparent adhesive tape, 3/4-inch wide, placed over the tube ends and perforated from the inside out with a needle, provided for aerodynamically clean conditions around the pressure sampling hole.

The use of HEXCEL stiffeners, as described in Fig. 8, prevented bulging and sagging of the screen matrix so that the flow geometry of the installed headers was in fact close to the design geometry. That such stiffeners were necessary can be seen from Fig. 18; a 0.1-inch bulge of the edge-supported screen pack, corresponding to a δZ of 0.05, could completely block the flow to the matrix in the region beyond $X = 0.85$. Some of the test results reported earlier, Ref. (1), were somewhat invalid because stiffeners were not used and screen bulging did indeed occur.

Calculation Methods

As described in the text, the measured $P(X)$ in both the inlet and exit headers were plotted as in Fig. 10. An average of the side-wall and broad-wall pressure readings was used to

fair in the li es. Close agreement between the two sets of $P(X)$ data taken at different z (or y) locations confirmed one of the key idealizations of the analysis, namely that pressure was a function of x only. These pressure lines allowed a direct reading for ΔP_{matrix} as a function of x. Then the $\sqrt{\Delta P_{matrix}}$ was used as being proportional to the velocity through the matrix v_m. Here it is implied that the matrix function factor is a constant. To the contrary, f varies as N_R to the - 0.34 power, as can be seen from the Table 3 entries, so that v_m varies as $\Delta P^{1/1.66}$ rather than $\Delta P^{1/2}$. The net effect of this correction is to increase the non-uniformity factors in Table 4 by 20 percent to 1.2 times the values reported. As this change is not considered to be significant in the present context it was not made.

Comparison of Predicted and Measured ΔP_{matrix}

In Table 3 a prediction for matrix pressure drop is presented. The ratio of test to predicted ΔP_{matrix} magnitudes is about 1.28 on the average (runs 50, 51 and 52 of Table 4). This discrepancy may be due to a combination of the following:

1. The estimated screen porosity of 0.725 may be in error. If it is 5 percent too high the predictions would be brought into agreement with the test values.
2. The stiffeners undoubtedly contribute a small percentage to the frictional drag and this was not allowed for in the calcul ions of Table 3.

Fig. II-1

Inlet headers showing the wooden inserts used to provide the shapes desired for the single-pass parallel and counter flow tests. See Table 1 and Figs. 18 and 19.

Fig. II-2

The return flow header for the two-pass parallel flow configuration. See Table 1.

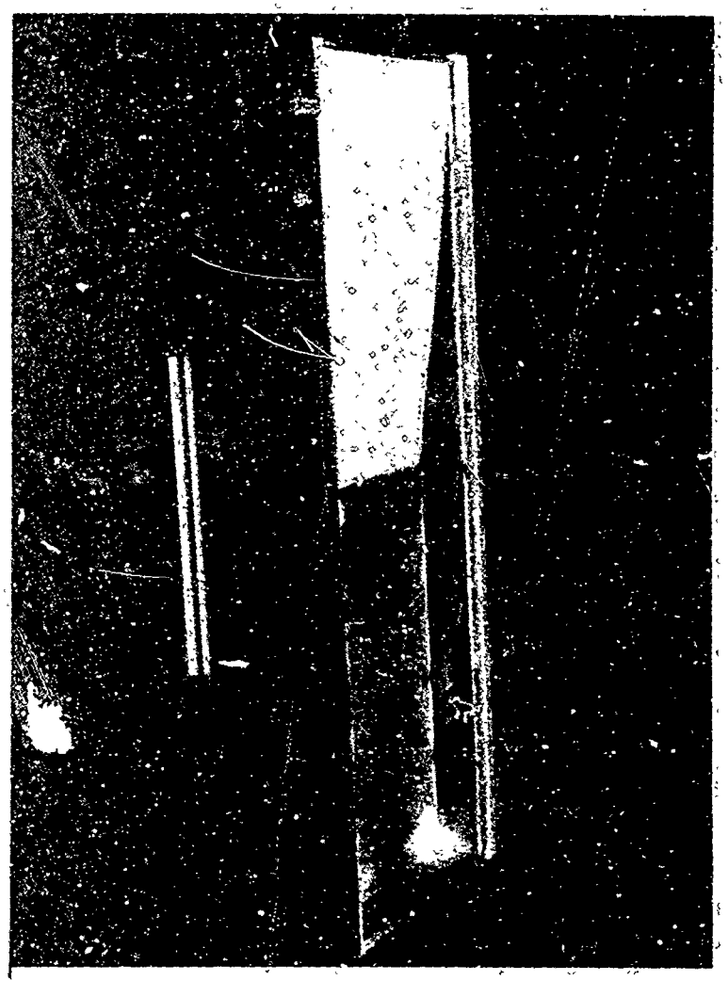

FIGURE II-2

FIGURE II-1

Aerojet-General Nucleonics
Foothoria Way
San Ramon, California
ATTN: Library

Aerojet-General Nucleonics
P.O. Box 77
San Ramon, Calif.
ATTN: Barbara Probert

AFOSR
ATTN: SREM
Washington 25, D.C.

Aro, Incorporated
AEDC Library
Arnold Air Force Stn.
Tennessee
ATTN: Tech. Files

Dr. A. P. Hatton
Mechanical Engineering Dept.
Manchester College of Tech.
Manchester, ENGLAND

AiResearch Mfg. Company
9851-9951 Sepulveda Blvd.
Los Angeles 45, California
Attn: Dr. John Mason

AiResearch Mfg. Company
9851-9951 Sepulveda Blvd.
Los Angeles 9, California
Attn: Mr. R.D. Mueller

AiResearch Mfg. Company
9851-9951 Sepulveda Blvd.
Los Angeles 9, Calif.
Attn: Dr. von der Nuell

Northern Res. & Engrg. Corp.
219 Vassar Street
Cambridge, Mass. 02139

AiResearch Mfg. Company
402 South 36th Street
Phoenix Arizona
Attn: Elmer Wheeler
Dept. 93-92

The Air Preheater Co.
Wellsville, N.Y., 14895
Attn: Engrg. Library

Allis-Chalmers Mfg. Co.
General Machinery Div.
Milwaukee 1, Wisconsin
Attn: Mr. R.C.Allen, Dir.
of Mech. Engrg.

Amer. Soc. of Heat/Refrig.
Air Cond. Engineers, Inc.
United Engrg. Center
345 E. 47th Street
New York 17, N.Y.

Amer. Soc. of Mech. Engrs.
United Engineering Center
345 East 47th Street
New York 17, New York
Attn: Mr. George D. Finster
Standards Manager

Dr. Aaron J. Friedland, Head
Engrg. Analysis Section
Atomic Power Dev. Assoc., Inc.
1911 First Street
Detroit, Michigan 48226

Argonne National Lab.
Library Services Dept.
Report Sect.-Bldg.14,Rm.14
9700 South Cass Avenue
Argonne, Illinois, 60440

Argonne National Labs
9700 South Cass Avenue
Argonne, Illinois, 60440
Attn: Dr. David Miller,
ISNE School

Argonne National Labs
9700 South Cass Avenue
Argonne, Illinois, 60440
Attn: Mr. M. Patrick

Office of the Asst.
Chief of Staff, G-4
Res. and Dev. Div.
Dept. of the Army
Washington 25, D. C.

U.S. Army Ord.Missile Cmd.
Redstone Arsenal, Alabama
Attn: AMSMI-RR,Bldg.5429

David Aronson
Worthington Air Con. Co.
Air Conditioning Div.
Ampere Station
East Orange, New Jersey

Atlantic Res. Corp.
Alexandria, Virginia
Attn: Dr. M.Markels, Jr.

U.S. Atomic Energy Com.
Div. of Tech. Info.Ext.
P.O.Box 62
Oak Ridge, Tennessee 37831

Atomics International
P.O. Box 309
Canoga Park, Calif.
Attn: Library

Atomic Power Dev.
Associated, Inc.
Detroit 26, Michigan
Attn: Dr. Wayne H. Jens

Auburn University
Dept. of Mech. Engrg.
Auburn, Alabama
Attn: Prof.D. Vestal,
Chairman

Avco Everett Res. Lab.
2385 Revere Beach Parkway
Everett 49, Mass.
Attn: Tech. Library

The Babcock & Wilcox Co.
Res. & Dev. Center
P. O. Box 835
Alliance, Ohio
Attn: Library

The Babcock & Wilcox Co.
Res. & Dev. Center
P.O. Box 835
Alliance, Ohio
Attn: C.P. Welch

Battelle Memorial Inst.
505 King Avenue
Columbus 1, Ohio
Attn: Dr. H.W.Russell

Dr. W. Bolley
4592 Via Vistoso
Santa Barbara, Calif.

C. F. Braun and Co.
Murray Hill, New Jersey
Attn: Mr. Earl Phillips

Brookhaven Nat. Lab.
Tech. Info. Division
Upton, Long Island, N.Y.
Attn: Res. Library

Mr. F. A. Brooks
Dept. of Agr. Engrg.
Univ. of Cal.Agr. Experiment
Station
Davis, California

Brown Boveri Corp.
19 Rector Street
New York N.Y. 10006
Attn: E. H. Stauffer
Staff Assistant

Brown Fintube Co.
300 Huron Street
Elyria, Ohio
Attn: Mr. John W.Brown Jr.

Prof. Harry Buchberg
Univ. of Cal at L.A.
Dept. of Mech. Engrg.
Los Angeles 24, Calif.

Univ. of Cal. at L.A.
Engrg. Dept.
Los Angeles 24, Calif.
Attn: Dean L.M.K.Boelter

University of Calif.
College of Engrg.
Berkeley 4, California
Prof. H.A.Johnson, M.E.

University of California
College of Engrg.
Berkeley 4, California
Attn: Prof. A.Oppenheim

Calif. Inst. of Tech.
Mech. Engrg. Dept.
1201 E. California St.
Pasadena 4, California

Calif. Inst. of Tech.
Mech. Engrg. Dept.
1201 E. California St.
Pasadena 4, California
Attn: Prof. B.H.Sage

University of California
College of Engrg.
Berkeley 4, California
Attn: Prof.R.A.Seban,M.E.

Calif. Research Corp.
576 Standard Avenue
Richmond, California
Attn: J.H.McPherson

Case Inst. of Tech.
Dept. of Mech. Engrg.
University Circle
Cleveland 6, Ohio
Attn: ProfJ.R.Moszynski

Caterpillar Tractor Co.
Peoria 8, Illinois
Attn: Mr. Lloyd E.Johnson
Assist. Dir. of Research

Caterpillar Tractor Co.
Peoria 8, Illinois
Attn: Mrs. M.M. Landuyt
Res. Lib.

The Catholic Univ. of Am.
Dept. of Mech. Engrg.
Washington 17, D.C.
Attn: Prof. J. Steffens

Chance-Vought Aircraft
Attn: Library
Dallas, Texas

Dr. D.L. Cochran
M & B Associates
P.O. 196
San Ramon, California

Prof. Alberto Coimbra
Escola Nacional de Quimica
Av. Pasteur 404
Rio de Janeiro, Brasil

University of Colorado
De.. of Mech. Engrg.
Boulder, Colorado
Attn: Prof. Frank Kreith

Columbia University
Heat Trans. Res. Lab.
632 W. 125th St.
New York 27, New York

Cooper Bessemer Corp.
Mt. Vernon, Ohio
Attn: R. L. Boyer
V.Pres. & Chief Engrr.

Cornell Aero. Lab.
4455 Genesee Street
Buffalo 21, New York
Attn: J.P.Desmond, Lib.

Cornell University
College of Engineering
Dept. of Heat Power Engrg.
Ithaca, New York
Attn: Prof. D. Dropkin

Mr. W. H. Comtois
129 Thornberry Drive
Pittsburgh 35, Pa.

Defense Docum. Center
Cameron Station
Alexandria, Virginia,22314

Mr. E. A. Drury
Thermodynamics Specialist
Gen. Dynamics/Astronautics
3634 Ben Street
San Diego, Calif. 92111

Dynatech Corp.
17 Tudor Street
Cambridge, Mass.

Eitel-McCullough, Inc.
301 Industrial Way
San Carlos, California
Attn: Tech. Library

Elliott Company
Jeannette, Pennsylvania
Attn: Dr. J. R. Shiels
Dev. Engrg. Dept.

NPFO, U.S.Army Engineer
Reactors Group
Ft. Belvoir, Va. 22060
Attn:Mr.Hadju, Sup.Staff
Engr Dept/NPFO Bldg T-2384

Engrg. Soc. Library
United Engrg. Trustees, Inc.
345 E. 47th Street
New York 17, N. Y.

Professor Darryl E. Metzger
Dept. of Mech. Engrg.
Arizona State University
Tempe, Arizona

Ferrotherm Company
1861 65th Street
Cleveland 3, Ohio
Attn: Mr. Sven Holm

Dr. Robert W. Fox
410 Club Lane
Lafayetter, Indiana

The Franklin Institute
Labs. for Research and
Development
Philadelphia 3, Pa.
Attn: Francis L. Jackson,
Director

Mr. K. A. Gardner
Engineering Department
The M W. Kellog Co.
711 Third Avenue
New York 17, N.Y.

Library
Gen. Dynamics/Gen.Atomic
P.O. Box 608
San Diego 12, California

General Electric Co.
Gen. Engineering Lab.
Schenectady 5, New York
Attn: D.H.Brown, Thermal
System Engrg.

Dr. F. A. Schraub
APED, Bldg. K, Rm. 14J
General Electric Company
San Jose, California

General Electric Co.
Research Lab.
P.O. Box 1088
Schenectady 5, New York

General Electric Co.
Main Library
Schenectady 5, New York 12305
Attn:Miss A. Ruane

General Electric Co.
1000 Western Ave.
West Lynn 3, Mass
Attn: Paul C. Setze
Bldg. 2-40

General Electric Co.
Atomic Power Equip. Div.
San Jose, California
Attn: W. A. Sutherland
P.O. Box 254

General Electric Co.
2151 So. 1st Street
Atomic Power Equip. Div.
San Jose, California
Attn: P. E. Tippets

General Motors Corp.
Harrison Radiator Div.
Lockport, New York
Attn: Mr. J. W. Godfrey

General Motors Corp.
Research Laboratories
12 Mile & Mound Roads
Warren, Michigan 48090
ATTN: Library, c/o R.W. Gibson

General Motors Corp.
Research Laboratories
12 Mile & Mound Roads
Warren, Michigan 48090
Attn: Mr. W. A. Turunen,
Engrg. Dev. Dept.

Mr. Ray L. Lyerly
So. Nuclear Engrg., Inc.
P.O. Box 578
Dunedin, Florida 33528

Gulf Res. & Dev. Co.
P.O. Drawer 2038
Pittsburgh, Pa. 15230
Attn: F. F. Kottcamp

International Harvester Co.
Engineering Research Dept.
5225 S. Western Blvd.
Chicago 9, Illinois
Attn: Dr. Simon K. Chen

Richard Herold, Pres.
Sulzer Bros., Ltd.
19 Rector Street
New York, N.Y. 10006

Edward Hines, Director
Engrg. Res. Dept.
The Detroit Edison Co.
2000 Second Ave.
Detroit 26, Michigan

Mr. Albert L. Holiday
114 Sharene Lane #4
Walnut Creek, Calif.

Prof. E. D. Howe, Dir.
Sea Water Conversion Lab.
University of California
1310 South 46th Street
Richmond, California

Illinois Inst. of Tech.
Dept. of Mech. Engrg.
Technology Center
Chicago 16, Illinois
Attn: Heat Transfer Lab.

University of Illinois
Mech. Engineering Dept.
Urbana, Illinois
Attn: Prof. S. L. Soo

M. W. Kellogg Co.
711 Third Avenue
New York 17, N. Y.
Attn: Mr. G.P.Eschenbrenn

M. W. Kellogg Company
711 Third Avenue
New York 17, N. Y.
Attn: F. W. Peterson

M. W. Kellogg Company
711 Third Avenue
New York 17, N. Y.
Attn: Ronald B. Smith
Vice President

Mr. R. V. Kleinschmidt
20 East Street
Stoneham 80, Mass.

Mr. S. Kopp, Manager
Nuclear Products Dept.
Struthers Wells Corp.
Warren, Pa.

The Kraissl Co., Inc.
229 Williams Avenue
Hackensack, New Jersey
Attn: F. Kraissl, Jr.

Prof. Shankar Lal
Dept. of Mech. Engrg.
University of Roorkee
ROORKEE, U.P., INDIA

Dr. Milton B. Larson
Dept. of Mech Engrg.
Oregon State College
Corvallis, Oregon

Mr. E. J. LeFevre
Dept. of Mech. Engrg.
Queen Mary College
LONDON E.1, ENGLAND

A. V. Lisin
SLAC
Stanford, California

Logan Lewis Library
Carrier Res. & Dev. Co.
Carrier Parkway
Syracuse, New York 13201

Lummus Company
146 Hayes Avenue
Newark, New Jersey
Attn: Stanley Grossel,
Process Engr.

Lockheed Aircraft Co.
Technical Library
Burbank, California
Attn: B.L. Messinger,
Engrg. N. 72.

R. E. Lundberg
Vidya Inc.
1450 Page Mill Rd.
Palo Alto, California

Mr. Frank L. Maier
156 Moraga Way
Orinda 1, California

Mass. Inst. of Tech.
Cambridge 39, Mass. 02139
Attn: Prof. W. H. McAdams
Chem. Engrg.

Mass. Inst. of Tech.
Cambridge 39, Mass. 02139
Attn: H. S. Mickley
Chem Engrg.

Mass Inst. of Tech.
Cambridge 39, Mass. 02139
Attn: W. M. Rohsenow
Mech. Engineering Rm 1-212

Mass. Inst. of Tech.
Cambridge 39, Mass. 02139
Attn: E. S. Taylor
Gas Turbine Lab.

McGraw-Hill Publishing Co.
330 West 42nd Street
New York 36, New York
Attn: L. N. Rowley, Editor
& Publisher, POWER

Dr. J. J. McMullen
17 Battery Place
New York 4, New York

University of Michigan
228 W. Engrg. Bldg.
Ann Arbor, Michigan
Attn: J. A. Clark

University of Minnesota
Mech. Engrg. Dept.
Minneapolis, Minnesota
Attn: D. R. G. Eckert

Prof. J. W. Mitchell
University of Wisconsin
Dept. of Mech. Engrg.
Madison 6, Wisconsin

Prof. R. W. Stuart Mitchell
Laboratorium voor Verbrandingsmotoren en Gasturbines
der Technische Hogeschool
Mekelweg 2
DELFT, HOLLAND

Modine Manufacturing Co.
1500 DeKoven Avenue
Racine, Wisconsin, 53401
Attn: Librarian

Morgantown Research Center
Bureau of Mines
Morgantown, West Virginia
Attn: Mr. J. P. McGee

Dr. Carl A. Moore, Jr.
1360 K Shadow Lane
Fullerton, Calif. 92631

NASA
Lewis Research Center
2100 Brookpark Road
Cleveland, Ohio 44135
Attn: Library (2)

NASA
Ames Research Center
Moffett Field, Calif.
Attn: Library

NASA
Langley Research Center
Langley Station
Hampton, Virginia, 23365
Attn: Library

Commanding Officer
Office of Naval Research
Branch Office
Navy No. 100
Fleet Post Office
New York, New York

SEND TO:

(25) Commanding Officer
Office of Naval Research
Branch Office
Keysign House
429 Oxford Street
London, W.1, ENGLAND

Office of the Asst. Naval Attache For Research
Naval Attache, Amer. Embassy
Navy No. 100, Fleet P.O.
New York, New York

SEND TO:

(1) Mr. A. J. Ede
Heat Division
Mech. Engrg. Res. Lab.
D.S.I.R., East Kilbride
near GLASGOW, SCOTLAND

Office of the Administrator
NASA Headquarters,
Washington D.C. 20546

Chief, Bureau of Ships
Department of the Navy
Washington 25, D.C.
Attn: Dir. of Research

Chief, Bureau of Ships
Department of the Navy
Washington 25, D. C.
Attn: Code 1500

Chief, Bureau of Ships
Department of the Navy
Washington 25, D.C.
Attn: Code 513

Chief of Naval Research
Department of the Navy
Washington 25, D.C.
Attn: Code 429 (2)

Chief of Naval Research
Dept. of the Navy
Washington 25, D.C.
Attn: Code 438

Chief, Bureau of Ships
Department of the Navy
Washington 25, D.C.
Attn: Code 651

U.S. Naval Postgrad. Sch.
Monterey, California
Attn: Library

Chief, Bur. of Aeronautics
Department of the Navy
Washington 25, D.C.
Attn: PP-22 (2)

Chief, Bureau of Ships
Technical Lib., Code 210 L
18th & Constitution Ave. N.W.
Washington D.C. 20025 (2)

Professor C. P. Howard
Bureau of Ships, Code 645
Dept. of the Navy
Washington 25, D.C.

Chief, Bur. of Aero.
Department of the Navy
Washington 25, D.C.
Attn: Aer-AE-651

Director
Naval Research Laboratory
Washington 25, D.C.
Attn: Code 2028 (6)

Chief, Bureau of Ships
Department of the Navy
Washington 25, D.C.
Attn: Code 550 (2)

Office of Naval Research
346 Broadway
New York 13, New York
Attn: Dr. Saul Berman

Chief Scientist
Office of Naval Research
Branch Office
1030 E. Green Street
Pasadena, California

Chief, Bureau of Ships
Department of the Navy
Washington 25, D.C.
Attn: Code 430 (2)

Office of Naval Research
Washington 25, D.C.
Attn: Mechanics Branch

U.S. Naval Postgrad. Sch.
Monterey, California
Attn: Prof. Paul Pucci

Chief, Bur. of Aero.
Department of the Navy
Washington 25, D.C.
Attn: PP-33 (2)

University of New Mexico
Dept. of Mech. Engrg.
Albuquerque, New Mexico
Attn: Prof. V.S.Skoglund

New York University
Dept. of Mech. Engrg.
University Heights
New York 53, N.H.
Attn: Prof. Fred Landis

R. H. Norris
Advanced Tech. Labs.
6th Floor, Bldg. 37
General Electric Co.
P.O. Box 11
Schenectady, N.Y. 12301

No. Amer. Aviation, Inc.
International Airport
Los Angeles 9, California
Attn: Mr. M.A.Sulkin

Oak Ridge National Lab.
Y-12 Tech. Lib.
P.O. Box Y
Oak Ridge, Tennessee 37831

Oak Ridge National Lab.
9204-1, Y-12
P.O. Box Y
Oak Ridge, Tennessee 37831
Attn: Mr. R. N. Lyon

Mr. A. J. Oberg
Senior Dev.Engrg.Ord. Div.
Minneapolis-Honeywell
600 North Second
Hopkins, Minnesota

Perfex Corporation
500 West Oklahoma Ave.
Milwaukee 7, Wisconsin
Attn: Mr. W. W. Schwid

R. C. Perpall
5433 Whitefox Drive
Palos Verdes Estates, Calif.

H. Phillips, Assoc.Dir.Res.
Foster Wheeler Corp.
110 So. Orange
Livingston, New Jersey

Princeton University
Princeton, New Jersey
Attn:Lib., J. Forrestal
Res. Center

Purdue University
School of Mech. Engrg.
Lafayetter, Indiana
Attn: Prof. D.S.Clark

Republic Aviation Corp.
Farmingdale, Long Island
New York
Attn: Library

Mr. D. W. Retzinger
Perfex Corporation
Heat Transfer Products
500 West Oklahoma Avenue
Milwaukee 7, Wisconsin

K. C. Rosenbert, Supervisor
Tech. Document Center
Hughes Aircraft Company
Florence and Teale Streets
Culver City, California
Attn: MS E-110

University of Santa Clara
Santa Clara, California
Attn: Prof. R. K. Pefley

Mr. L. P. Saunders
P. O. Box L
Carmel California

Mr. Wolfgang Schaechter
Space Nuclear Propulsion Off.
Albuquerque Extension
U.S. Atomic Energy Commission
P.O. Box 5400
Albuquerque, New Mex. 87115

Mr. David M. Schoenfeld
Mariomi Road
New Canaan, Conn.

Prof. F. L. Schwartz
Dept. of Mech. Engrg.
University of Florida
Gainsville, Florida

Shell Development Co.
Emeryville, California
Attn: Dr. C. R. Carbett

Librarian
Shell Development Co.
Emeryville, Calif.

Lear Siegler, Inc.
Engineering Library
P. O. Box 6719
Cleveland 1, Ohio

Mr. Edward Simons
27 Sunnyside Avenue
Mill Valley, Calif. 94943

Solar Aircraft Co.
San Diego 12, Calif.
Attn: Mr. P. A. Pitt (2)
Vice Pres. Engrg/Res.

Solar
Attn: Librarian
2200 Pacific Highway
San Diego, Calif. 92112

Space Tech. Lab., Inc.
Mechanics Division
Space Tech. Center
One Space Park
Redondo Beach, Calif.
Attn: Neal Lansing

Mr. S. B. Spangler, Jr.
275 Valley Street
Los Altos, California

Dr. B. I. Spinrad
Argonne Nat'l. Lab.
Reactor Physics Div.
Bldg. 208
9700 South Cass Avenue
Argonne, Illinois, 60440

Stanford Research Inst.
Menlo Park, California
Attn: Mr. S. H. Clark
Industrial Econ. Div.

Stanford University
Stanford, California
Attn: Dean J. M. Pettit
Sch. of Engrg.

Stanford University
Stanford, California
Attn: Engrg Lib (2)

Stewart-Warner Corp.
1514-Drover Street
Indianapolis 7, Indiana
Attn: Library

Mr. Richard L. Stone
William Wallace Co.
Belmont, California

SVERDRUP/PARCEL and Assoc.
915 Olive Street
St. Louis Missouri 63101

Sylvania Elec.Prod.Inc.
Lib.Electron. Def. Lab.
P.O. Box 205
Mountain View, California

Syracuse University
Syracuse 10, New York
Attn: Ralph M. Watson
Assoc. Dean of Engrg.

Y. S. Tang, Dept. 7897
Allison Division
Gen. Motors Company
Indianapolis, Indiana

David Taylor Model Basin
Aero. Lab.
Washington 7, D.C.
Attn: Library

Texas E. Transmn. Corp.
P. O. Box 1612
Shreveport, Louisiana
Attn: Mr. C. W. Marvin

The Trane Company
LaCrosse, Wisconsin
Attn: W. C. Dackis

The Trane Company
LaCrosse, Wisconsin
Attn: Mr. H. C. Rooks (2)

The Trane Company
La Crosse, Wisconsin
Attn: Mr. I. T. Wetzel

Tufts University
Mech. Engrg. Dept.
Medford, Mass. 02155
Attn: Dr. Trefethen

Unified Science Associates
926 S. Arroyo Parkway
Pasadena, California
Attn: S. Naiditch

United Aircraft Corp.
400 Main Street
East Hartford 8, Conn.
Attn: H. D. Rix
Chief, Lib. System

Union Carbide Nuclear Co.
Oak Ridge Gaseous Dif.Plant
Plant Records Dept.
P.O. Box P (2)
Oak Ridge, Tennessee 37831

Vidya, Div. Itek Corp.
1450 Page Mill Road
Palo Alto, California
Attn: D. E. Abbott

Vidya, Div. Iteck Corp.
1450 Page Mill Road
Palo Alto, California
Attn: D. C. Briggs

Vidya Div. Itek Corp.
1450 Page Mill Road
Palo Alto, California
Attn: L. McLaughlin
Librarian

Vidya Div. Iteck Corp.
1450 Page Mill Road
Palo Alto, California
Attn: M. W. Rubesin

Virginia Polytechnic Inst.
Blacksburg, Virginia
Attn: Carol N. Newman
Library

Vitro Laboratories
200 Pleasant Valley Way
West Orange, New Jersey
Attn: Library

Professor M. A. Saad
Department of Mech. Engrg.
University of Santa Clara
Santa Clara, California

Engineering Library
213 Guggenheim
University of Washington
Seattle, Wash. 98105

Dr. N. A. Weil
Cummins Engine Co.
1000 5th Street
Columbus, Indiana

Westinghouse Elect. Corp.
Lester Branch P. O.
Philadelphia 13, Pa.
Attn: Mr. F. K. Fisher,
Mgr. Dev. Engrg.

Westinghouse Elect. Corp.
Bettis Atomis Power Lab.
P. O. Box 1468
Pittsburgh 30, Pa.
Attn: Technical Library

Westinghouse Elec. Corp.
306 4th Avenue
Pittsburgh, Pa.
Attn: Library

Westinghouse Elect. Corp.
Research Laboratory
Beulah Road
Pittsburgh 35, Pa.
Attn: Dr. Stewart Way

Prof. of Ordinance
U.S. Military Academy
West Point, New York

University of Wisconsin
1513 University Ave.
Madison 5, Wisconsin
Attn: Prof. E. Obert

Wolverine Tube Division
17200 Southfield Road
Allen Park, Michigan
Attn: Mr. J.Eddens

Mr. Stanley Wong
1128 West 126th Street
Los Angeles, Cal. 90044

Dr. Roger M. Wright
AiResearch Mfg. Co.
9851 Sepulveda Blvd.
Los Angeles 9, Calif.

Inst. of Tech. Lib.
MCLI-LIB, Bldg. 125,Area B
Wright-Patterson AFB
Ohio

Technical Library
AiResearch Mfg. Div.
Garrett Corporation
9851-9951 Sepulveda Blvd.
Los Angeles 9, Calif.
ATTN: Kenneth R. Brown

ARL (AFRO)
Wright-Patterson AFB
Ohio
Attn: RRLA Library

AMC
Wright-Patterson AFB
Ohio
Attn: Library

Wright Air Dev. Center
Wright-Patterson AFB
Ohio
Attn: WCREO-2

Young Radiator Company
709 S. Marquette Street
Racine, Wisconsin
Attn: Mr. H. F. Brinen,
V.Pres.& Exec. Engr.

Mr. A. Topouzian
Gas Turbine Dept.
Ford Motor Co.
20,000 Rotunda Dr.
Dearborne, Michigan

Prof. W. T. Sawyer, Head
Dept. of Mech. Engrg.
The Catholic University
Washington D. C. 20017

Mrs. Rachel MacDonald
Eng-Staff Library
Ford Motor Company
Dearborne, Michigan

Mrs. L. B. Phillips, Suptdt.
Tech. Info. Sec.
Scientific Lab.
Ford Motor Company
Dearborne, Michigan

Ivan Swatman, Eng. Staff
Gas Turbine Dept.
Ford Motor Co.
20,000 Rotunda Drive
Dearborne, Michigan

W. A. Compton
Assistant Director of Res.
SOLAR
2200 Pacific Highway
San Diego, Calif. 92112

Mr. Chris Hazeloop
Senior Project Engineer
Advanced Engineering
Perfex Corporation
500 West Oklahoma Avenue
Milwaukee, Wisc. 53207

The Trane Company
LaCrosse, Wisconsin
ATTN: Mr. R. L. Webb